Nucleic Acids Research, 2017 **1**
doi: 10.1093/nar/gkx698

Model-based design of RNA hybridization networks implemented in living cells

Guillermo Rodrigo[1,2,†], Satya Prakash[3,†], Shensi Shen[1], Eszter Majer[2], José-Antonio Daròs[2] and Alfonso Jaramillo[1,3,4,*]

[1]Institute of Systems and Synthetic Biology, Université d'Évry Val d'Essonne—CNRS, F-91000 Évry, France, [2]Instituto de Biología Molecular y Celular de Plantas, CSIC—Universidad Politécnica de Valencia, 46022 Valencia, Spain, [3]Warwick Integrative Synthetic Biology Centre and School of Life Sciences, University of Warwick, Coventry, CV4 7AL, UK and [4]Institute for Integrative Systems Biology (I2SysBio), University of Valencia-CSIC, 46980 Paterna, Spain

Received May 17, 2017; Revised July 19, 2017; Editorial Decision July 26, 2017; Accepted July 27, 2017

ABSTRACT

Synthetic gene circuits allow the behavior of living cells to be reprogrammed, and non-coding small RNAs (sRNAs) are increasingly being used as programmable regulators of gene expression. However, sRNAs (natural or synthetic) are generally used to regulate single target genes, while complex dynamic behaviors would require networks of sRNAs regulating each other. Here, we report a strategy for implementing such networks that exploits hybridization reactions carried out exclusively by multifaceted sRNAs that are both targets of and triggers for other sRNAs. These networks are ultimately coupled to the control of gene expression. We relied on a thermodynamic model of the different stable conformational states underlying this system at the nucleotide level. To test our model, we designed five different RNA hybridization networks with a linear architecture, and we implemented them in *Escherichia coli*. We validated the network architecture at the molecular level by native polyacrylamide gel electrophoresis, as well as the network function at the bacterial population and single-cell levels with a fluorescent reporter. Our results suggest that it is possible to engineer complex cellular programs based on RNA from first principles. Because these networks are mainly based on physical interactions, our designs could be expanded to other organisms as portable regulatory resources or to implement biological computations.

INTRODUCTION

Synthetic biology offers the possibility of engineering a large variety of functional circuits *in vivo* (1–4), such as transcriptional control circuits implementing sophisticated digital behaviors (4). In this regard, RNA has also recently emerged as a substrate of choice to engineer new regulatory mechanisms, due to its high functional versatility and programmability (5–8). Natural or synthetic regulatory RNAs are now used for purposes other than the direct control of certain target genes (8,9), with the aim of implementing complex behaviors in the cell too. However, more work is needed in this direction, especially to implement cascades and feedback loops (1–4) only with RNA. To this end, we require post-transcriptional mechanisms mimicking the combinatorial action achieved by transcription factors (proteins) landing on promoter regions (DNA), as well as mechanisms to store and retrieve information through RNA molecules without the participation of DNA (i.e. RNAs with different functional states).

To address this problem, here we designed and implemented *in vivo* RNA hybridization networks, i.e. networks of RNA molecules with multiple interaction domains that can be reconfigured through hybridization events (in *trans*). Previous work on the design of synthetic regulatory RNAs *in vivo* has led to different ways of transferring information from small RNAs (sRNAs) to gene expression, such as those based on RNA regulators (5,6,8,10–15), riboswitches (16–18) and ribozymes (19–22). The use of RNA hybridization networks *in vivo* extends such works by developing RNA mediators in such information transference (RNA regulation of the RNA regulator), something instrumental to increase the regulatory power of the system and previously achieved *in vitro* (7,9,23,24).

To implement an RNA hybridization network in *Escherichia coli*, we assumed that (i) RNA–RNA interactions are initiated by non-hybridized complementary regions called toeholds (5,6); (ii) the ribosome-binding site (RBS) of a given messenger RNA (mRNA), or even the translation start site (6,13), can be considered a type of

*To whom correspondence should be addressed. Tel: +44 24 765 73432; Email: Alfonso.Jaramillo@synth-bio.org
†These authors contributed equally to this work as first authors.

toehold mediating the interaction with the 16S ribosomal RNA; (iii) RNA-RNA interactions can simply be explained by 2D energetic features (5,25); and (*iv*) the assembly of multiple RNA strands is mostly hierarchical (7,24). We then exploited physicochemical RNA models (26–29) to predict the different stable conformational states and free energy levels of the network. Such predictability allows for the design of novel gene circuits based on RNA with sophisticated functionalities, as done with DNA strands *in vitro* (30–32).

We focused on the particular case of a linear network implemented by RNAs with two interaction domains (i.e. an RNA hybridization chain reaction) (7) and that results in the activation of gene expression (output). Initially, the conformational state of given RNA corresponds to the OFF state, where the domain to interact with an upstream RNA (trigger RNA) is active, and the domain to interact with a downstream RNA (target RNA) is inactive (*cis*-repressed). Upon interaction with the trigger RNA, the domain to interact with the target RNA becomes active (ON state). In this article, we first present a general computational model for creating RNA hybridization networks. We then present the design of five minimal networks as a proof-of-concept of the approach. We finally show several experimental results that prove that these networks are functional at the molecular and cellular levels, which validate the predictability of the model.

MATERIALS AND METHODS

RNA sequence design

We exploited a thermodynamic model to design cascades of regulatory RNAs to finally control gene expression. The system is composed of three different RNA species: two sRNAs and one 5′ untranslated region (UTR). We constructed an objective function based on free energies and RNA structures (Supplementary Figure S1), which were calculated thanks to a physicochemical model (26,27). In particular, this involved the energies of activation and hybridization corresponding to the interaction between the two sRNAs and the energies of activation and hybridization corresponding to the interaction between the sRNA complex and the 5′ UTR (see more details in Supplementary Information). The objective function also accounted for the degree of occlusion and exposure of the RBS within the 5′ UTR intramolecular and intermolecular structures.

We applied a Monte Carlo simulated annealing optimization algorithm (33) to perform the *de novo* sequence design. Rounds of random mutations were applied and selected with such energy-based objective function (Supplementary Figure S2), an empirical linear function that integrates all energetic contributions to the intended regulatory behavior and that must be minimized. For that, we extended a previously reported algorithm for RNA design (5,25). We used the Vienna RNA package (26) for energy and structure calculations. The sequences of the riboregulators engineered in this work, as well as their cognate 5′ UTRs, are shown in Supplementary Table S1.

Plasmid construction

The different sRNA systems were chemically synthesized (IDT) and cloned in a pSTC2-based plasmid that contained a pSC101m replication origin (a mutated pSC101 ori giving a high copy number; E93K in *repA*) and a kanamycin resistance marker (Supplementary Figure S3). The pSTC2 vector, used in our previous works (22), has a superfolder green fluorescent protein (sfGFP) (34) as reporter gene, with a *ssr*A degradation tag (35) for fast turnover. The promoters P_{LlacO1} and P_{LtetO1} (36) control the expression of the two sRNAs, whereas the mRNA (containing the 5′ UTR) is constitutively expressed from promoter J23119. Strains and plasmids used in this study are listed in Supplementary Table S2.

Cell culture and reagents

Escherichia coli strain DH5α (Invitrogen) was used for plasmid construction purposes as described in the manual (37). Characterization experiments were performed in *E. coli* DH5α-Z1 cells (Clontech) or in *E. coli* K-12 MG1655-Z1 cells (both $lacI^+$ $tetR^+$) for control over the promoters P_{LlacO1} and P_{LtetO1} (the Z1 cassette produces LacI and TetR proteins (36)). As external inducers, we used isopropyl-β-D-thiogalactopyranoside (IPTG) and anhydrotetracycline (aTc). For characterization in a fluorometer (TECAN) or in a flow cytometer, plasmids carrying systems trigR11, trigR1 and trigR2 were transformed into DH5α-Z1 cells, while plasmids carrying systems trigR31 and trigR32 were transformed into MG1655-Z1 cells. Moreover, the plasmid carrying system trigR2 was transformed into MG1655-Z1 cells for characterization in a microfluidic device.

Cells were grown aerobically in LB or in M9 minimal media, prepared with M9 salts (Sigma-Aldrich), glycerol (0.8%, vol/vol) as the only carbon source, $CaCl_2$ (100 μM), $MgSO_4$ (2 mM), and $FeSO_4$ (100 μM). The kanamycin concentration was 50 μg/mL. Cultures were grown overnight at 37°C and at 225 rpm from single-colony isolates before being diluted for *in vivo* characterization. 1 mM IPTG (Thermo Scientific) was used for full activation of promoter P_{LlacO1} when needed, and 100 ng/ml aTc (Sigma-Aldrich) was used for full activation of promoter P_{LtetO1}. For microfluidic cultures, cells were grown aerobically in fresh LB and in LB supplemented with 0.05% sulforhodamine B (Sigma-Aldrich), and IPTG + aTc (i.e. we used sulforhodamine B to monitor the presence of inducers in the chamber) (22).

In vitro RNA–RNA interaction

To perform the *in vitro* transcription, 3 μg of each pUC18-derived plasmid (see details in Supplementary Information) was digested with Eco31I, and purified with silica-based columns (Zymo). We used approximately 1 μg of digested plasmid in the reaction. This was in 20 μl: 10 μl of plasmid, 2 μl buffer 10× (Roche), 0.4 μl DTT 10 mM, 1 μl NTPs 10 mM (Thermo Scientific), 0.5 μl Ribolock (40 U/μl, Thermo Scientific), 1 μl inorganic pyrophosphatase (0.1 U/μl, Thermo Scientific), 1 μl T7 RNA polymerase (50 U/μl, Epicentre) and 4.1 μl H_2O. We incubated the mix for 1 h at 37°C, and then added 20 μl of loading buffer with

formamide. The samples were heated at 95°C for 1.5 min, then cooled on ice, and then separated by electrophoresis (200 V, 2.5 h) in a 10% polyacrylamide gel, containing 8 M urea, TBE (1×). We cut the bands corresponding to the full-length RNAs for purification. The presence of RNA was confirmed by loading a small part of the purified preparations in another polyacrylamide gel.

For the reaction of RNA–RNA interaction, we used ∼20 ng of RNA for each of the transcripts. The buffer of the reaction was 50 mM Tris–HCl pH 7.5, 10 mM $MgCl_2$, 20 mM NaCl. The mix (20 μL) was denatured (1.5 min at 95°C) and slowly cooled (15 min at room temperature) (38). We then added 1.5 μl glycerol (87%) and 0.2 μl bromophenol blue–xylene cyanol (100×) to load the gel (15% polyacrylamide, buffer TAE, 1 mm thick), which was run for 2 h at 75 mA at 4°C. The gel was stained first with ethidium bromide and then with $AgNO_3$. We used the DNA molecular weight marker XIII (50 bp ladder, Roche).

ImageJ was used to quantify the bands (39), which are assumed to be proportional to mass. The apparent dissociation constants were calculated by translating the mass fractions into molar fractions with the molecular weight of the RNAs (see details in Supplementary Information).

Fluorescence quantification

Cells were grown overnight in LB medium and were then refreshed by diluting 1:200 in M9 medium. They were grown for additional 2 h to then load 200 ml in each well of the plate (Custom Corning Costar). Appropriate inducers (none, aTc, IPTG, or aTc + IPTG) were introduced when needed during refreshing. The plate was incubated in an Infinite F500 multi-well fluorometer (TECAN) at 37°C with shaking. It was assayed with an automatic repeating protocol of absorbance measurements (600 nm absorbance filter) and fluorescence measurements (465/35 nm excitation filter—530/25 nm emission filter for sfGFP) every 15 min. All samples were replicated on the plate from three different colonies.

Normalized fluorescence was obtained by subtracting the background values corresponding to M9 medium (in both fluorescence and absorbance values) and then dividing fluorescence by absorbance at $OD_{600} \approx 0.5$ (22). Corrected normalized fluorescence was obtained by subtracting the fluorescence of plain cells (autofluorescence).

Single-cell microfluidic analysis

The design of our microfluidic device was performed in AUTOCAD (AUTODESK), and it was already applied to study a synthetic genetic oscillator (40). All images were acquired using Zeiss Axio Observer Z1 microscopy (Zeiss). The microscope resolution was 0.24 μm with Optovariation 1.6×, resulting total magnification 1600× for both bright field and fluorescent images. Images were analyzed with MATLAB (MathWorks). Cells were tracked by defining a cell-to-cell distance matrix and the cell lineages were reconstructed. Finally, the fluorescence level of each cell in each fluorescence frame was extracted (see Supplementary Figure S4 for the setup).

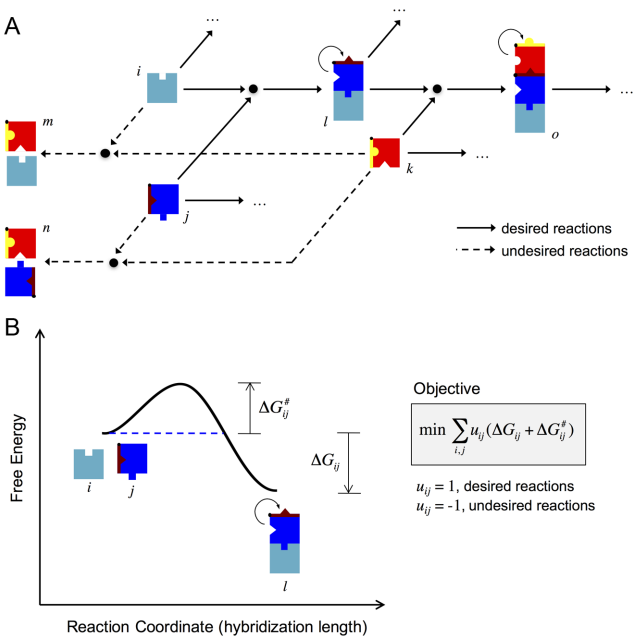

Figure 1. (**A**) General scheme of an RNA hybridization network implemented with RNA-triggered riboregulators (i.e., riboregulators that allosterically switch from an OFF state to an ON state upon interaction with another riboregulator; colored boxes with notches). The arrows indicate the possible hybridization reactions; solid lines for desired interactions (energetically favorable) and dashed lines for undesired interactions (energetically unfavorable). (**B**) Energy landscape of a particular reaction within the network (between the molecules *i* and *j*). This shows the different conformational states and their free energy levels as a function of a reaction coordinate (number of intermolecular base pairs). A general objective function, which should be minimized, is shown. The terms ΔG_{ij} and $\Delta G^{\#}_{ij}$ correspond to the free energies of hybridization and activation, respectively. Note that the free energy of hybridization is a negative magnitude, whereas the free energy of activation is a positive magnitude.

Flow cytometry analysis

Cells were grown overnight in LB medium and were then diluted 1:200 in fresh LB medium containing inducers (none, aTc, IPTG, or aTc + IPTG) and incubated to reach an OD_{600} of 0.2–0.4. Afterward, cells were diluted again in 1 ml PBS. All expression data were analyzed using a Becton-Dickinson FACScan flow cytometer with a 488 nm argon laser for excitation and a 530/30 nm emission filter (sfGFP). Gene expression of each sample was obtained by measuring the fluorescence intensity of thousands of cells. The data were analyzed using the Cytobank webserver by gating the events using scatter ranges, and then fluorescence histograms (without subtracting autofluorescence) plotted with MATLAB.

RESULTS

Thermodynamic model of RNA hybridization networks

We built a coarse-grained model, based on energies and structures, to describe the dynamic behavior a network consisting of an arbitrary number of different RNA molecules that can interact with each other (Figure 1A). Each node in the network is an individual species or a complex. The energy landscape associated with a given interaction (between

nodes *i* and *j*) is shown in Figure 1B. The reaction coordinate was defined as the number of intermolecular hydrogen bonds (or base pairs) between the two RNA molecules. In the energy landscape, one barrier (the free energy of activation; $\Delta G^{\#}_{ij}$) impinges on the progression of the reaction (41). This is associated with the degree of exposure of the toeholds to the solvent, and it has to be low to permit the initiation of the reaction (kinetic aspect). In addition, for an efficient reaction, the free energy of hybridization (ΔG_{ij}) has to be as negative as possible to ensure irreversibility in the intermolecular interaction (this represents the thermodynamic aspect of the reaction).

Following this model, it is possible to design a given RNA hybridization network by specifying a set of desired and undesired interactions. The nucleotide sequences of the different RNAs can be obtained by minimizing/maximizing the objective free energy ($\Delta G_{ij} + \Delta G^{\#}_{ij}$) of desired/undesired interactions (Supplementary Figure S1). Consequently, we developed a computational workflow to automate the network design process (Supplementary Figure S2), although a rational design could also be possible. In particular, we applied heuristic optimization (5) using Vienna RNA (26).

Design of RNA hybridization networks coupled to gene expression

We applied this thermodynamic model to guide the design of a simple network consisting in a chain reaction of three RNA molecules, together with the ribosome, as a proof-of-concept. Figure 2A illustrates this cascade (see also Supplementary Figure S5 where we detail the corresponding energy landscape). The first molecule is an sRNA that we call a signal riboregulator (SR). This molecule can interact with a second molecule, another sRNA called an SR-triggered riboregulator (SRR), which is initially in the OFF state (i.e., with a hidden/inactive toehold to interact with the downstream element). The resulting complex (SRR*), which is in the ON state (i.e. with the aforementioned toehold exposed/active), can subsequently interact with a third molecule, called an SRR-triggered riboregulator (SRRR). This strategy could facilitate the creation of larger cascades at the post-transcriptional level. For the purpose of designing a network to control gene expression, we considered SRRR to be the expression platform, i.e., a *cis*-repressed 5′ UTR of a given mRNA (see Supplementary Information for a rationale about the interaction with the ribosome).

By calculating the objective free energy ($\Delta G_{ij} + \Delta G^{\#}_{ij}$) for each interaction, we can evaluate if a set of three arbitrary RNA molecules follows the energetic/structural requirements. In this work, we designed five different riboregulatory cascades: trigR31, trigR32, trigR1, trigR2, and trigR11 (see complete sequences in Supplementary Table S1). Figure 2B illustrates the implementation of system trigR2. One of the toeholds that nucleates the interaction between SRR* and SRRR is hidden within the unhybridized structure of SRR. However, both toeholds that nucleate the interaction between SR and SRR are exposed (active) within their respective unhybridized structures. This ensures that the hybridization reaction between SR and SRR can occur. As a result, within the hybridized structure of SRR*, the toehold that nucleates the interaction with SRRR becomes active. Supplementary Figure S6 shows the sequence-structure schematics of all these systems (only the toehold sequences are shown for simplicity), where different interaction modes can be identified (i.e. different toehold positions and different intermolecular complex structures).

We followed different strategies to obtain the sequences implementing these systems using the same thermodynamic model. Systems trigR31 and trigR32 were obtained by sequential design, i.e. first designing the sequences of SR and SRR, and then the sequence of SRRR. The sequences of SR and SRR of these systems were based on previous riboregulatory elements taken from (6) (see sequence design details in Supplementary Information). Then, we computationally designed the corresponding SRRRs. By contrast, systems trigR1 and trigR2 were obtained by full design, i.e., designing the sequences of SR, SRR and SRRR at the same time. System trigR1 was obtained by specifying the unhybridized structures of SR and SRR, while for system trigR2, the hybridized structure of SRR* was specified (introduced, in both cases, as sub-objectives in the global objective function and not as enforced constraints). These specifications, although not functionally required, were introduced to prevent premature degradation of unstructured sRNAs. Finally, the sequences of system trigR11 were based on our previously published riboregulatory system RAJ11 (5). We split the sRNA into two halves (SR and SRR), and considered the cognate 5′ UTR as SRRR (Supplementary Figure S7). This resulted in a system based on the formation of a three-way junction (see sequence design details in Supplementary Information).

Because the sequences were selected only according to energetic criteria, the designed systems present different implementations in terms of toehold position within the structures. Indeed, we recognized active toeholds in the unpaired 5′ end (SRR of trigR31 and trigR32; SRRR of trigR31), in a loop (SR of trigR1, trigR2 and trigR11; SRR of trigR1 and trigR11; SRRR of trigR32, trigR1, trigR2 and trigR11), and in an inter-stem space (SR of trigR31 and trigR2; SRR of trigR2). This stresses the high designability of RNA hybridization networks.

Characterization of RNA hybridization networks at the population level

To test the functionality of our computational designs *in vivo*, the RNA systems were implemented as separate transcriptional units (with their respective promoters and terminators) in plasmids (Supplementary Figure S3, Table S2). These were then electroporated into *E. coli* cells expressing the transcriptional repressors LacI and TetR (see Materials and Methods; Figure 3A illustrates the engineered RNA circuit). We used P_L-based inducible promoters (36) for controlling the expression of SR and SRR with the external inducers isopropyl-β-D-thiogalactopyranoside (IPTG) and anhydrotetracycline (aTc), respectively. We used a superfolder green fluorescent protein (sfGFP) (34) with a degradation tag as the output for the circuits, because its fast maturation and degradation allows a better correlation between fluorescence and gene expression (especially in time-dependent experiments). Figure 3B shows the dynamic ranges (characterized by bulk fluorometry) of the en-

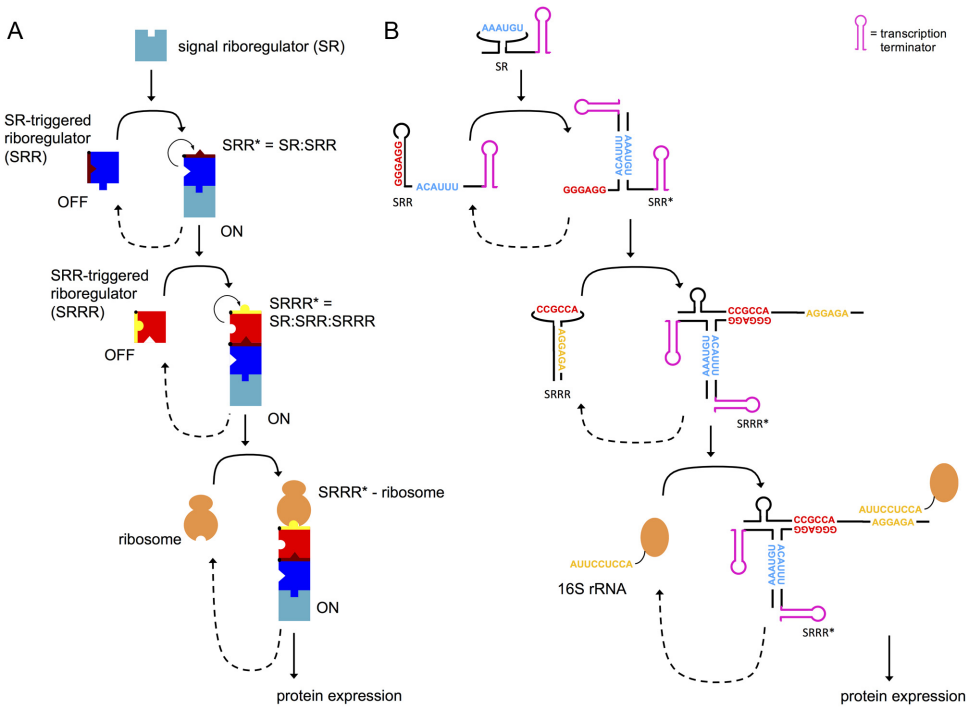

Figure 2. (**A**) Scheme of the simplest theoretical form of an RNA hybridization network, a chain reaction. (**B**) Sequence-structure schematics of a designer chain reaction (system trigR2). The toehold sequence for the interaction between the two sRNAs (SR and SRR) is shown in blue, and the toehold sequence for the interaction between the heterodimer (sRNA complex) and the 5′ UTR (SRRR) is shown in red. In the 5′ UTR, the RBS (shown in yellow) functions as a kind of toehold to interact with the ribosome.

gineered systems, probing the regulation of gene expression in living cells with two interacting sRNAs, as well as the versatility of the toeholds within different structural contexts. We also observed that the expression platforms (SRRRs) in systems trigR11 and trigR1 exert a much tighter control of the OFF state than those in the other systems (trigR2 being the one with the highest expression levels). Subsequently, we assessed the statistical significance of the reported activation folds. We found, for all systems, that the increase in fluorescence in response to both inducers (leading to the formation of complex SRRR*) is significantly greater than the increase in fluorescence induced by either IPTG or aTc individually (one-tailed Welch t-test, $P < 0.05$; Figure 3B). We also found, for systems trigR11, trigR1, and trigR2, that the sum of individual increases in fluorescence with IPTG and aTc is significantly smaller than the increase with both inducers (one-tailed Welch t-test, $P < 0.05$; Figure 3B). We thus confirmed the model-based designability of RNA hybridization networks.

In addition, we investigated the effects of some of the attributes defining the molecular implementation of the systems. In terms of stationary behavior, it is expected that the stability of the output protein does not modify substantially the activation fold (42). We characterized system trigR11 with a stable and unstable sfGFP, as this system shows one of the lowest expression levels, obtaining a slightly higher dynamic range with the more stable variant (Supplementary Figure S8). Also, the formation of the trimeric complex (SRRR*), and then sfGFP expression, greatly depends on the strength of the promoters that express the RNAs (43), as the dissociation constants between synthetic RNAs that hybridize are high (see below). We characterized the graded response of system trigR2 with IPTG and aTc, showing this dependence (Supplementary Figure S9). Finally, synthetic RNAs do not exploit the intricate cellular machinery. We introduced an Hfq target site in SRR (sequence MicF-M7.4 from (44)) to ask if the activation fold would be higher, as this RNA chaperone has a key role in post-transcriptional regulation (45). Using the system trigR31, as it exhibits the less digital behavior, we did not find an enhancement (Supplementary Figure S10A; see Supplementary Information for a rationale).

Probing the orthogonality between RNA-triggered riboregulators

Next, we performed an experimental study to assess the specificity of our designed sRNAs, using the systems trigR11 and trigR2 (Figure 4A and D). We chose these two systems because they seem to have the highest expression levels, what might favor a problem of cross-regulation when both systems work in the same cell. For this analysis, we constructed two new, crossed systems: one with the sRNAs (SR and SRR) from trigR2 and the 5′ UTR (SRRR) from trigR11 (Figure 4B), and the other with the sRNAs from trigR11 and the 5′ UTR from trigR2 (Figure 4E). The same promoters were used (P_L-based inducible promoters for the sRNAs, and a constitutive promoter for the mRNA). Computational simulations of cofolding using Vienna RNA (26) indicated that there is no significant free energy gap to promote hybridization between SRR* and SRRR if they are non-cognate pairs. When we tested this experimentally, we

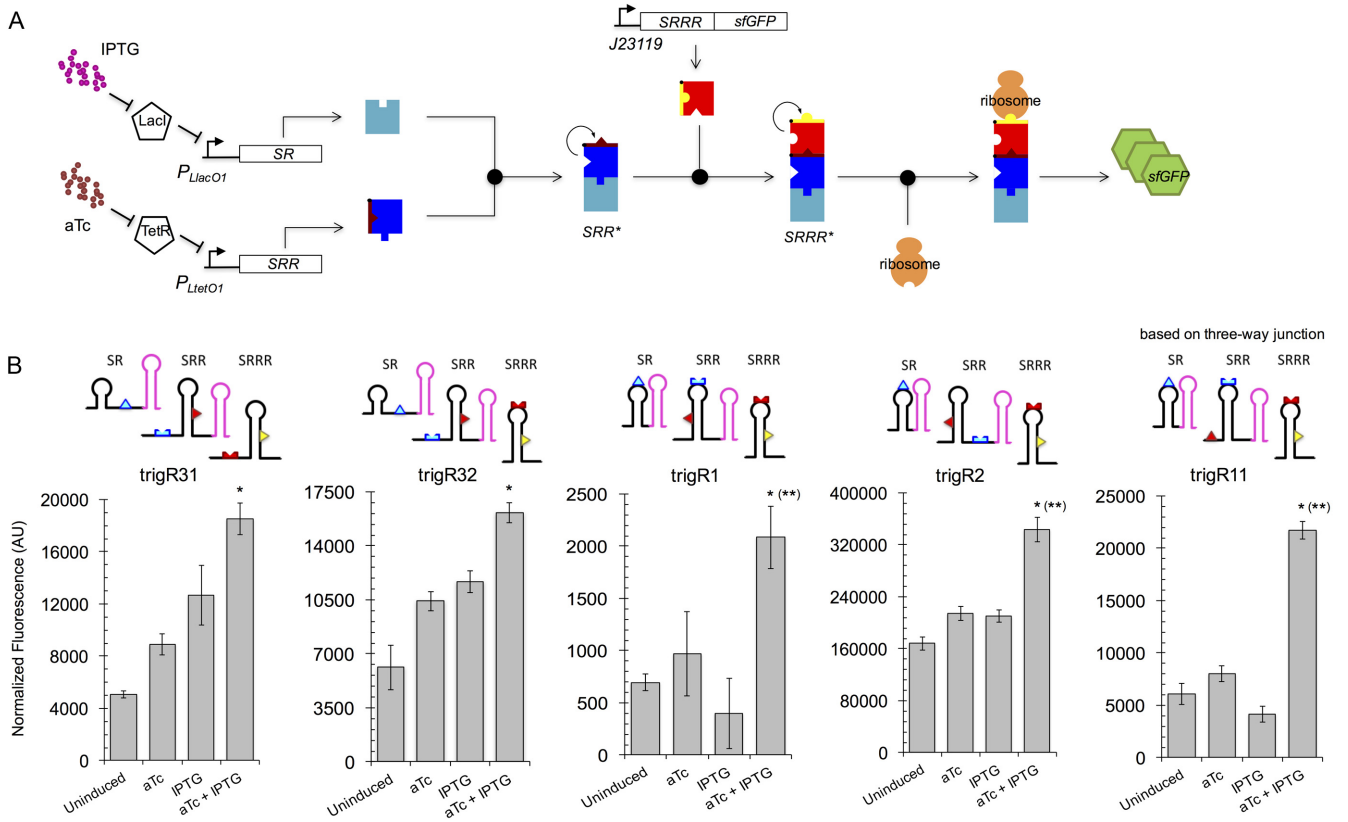

Figure 3. Functional characterization of designer RNA hybridization networks in bacterial cell populations. (**A**) Scheme of the engineered sRNA circuit. Promoters P_{LlacO1} and P_{LtetO1} control the expression of the two sRNAs (SR and SRR), which can be tuned with different concentrations of the external inducers IPTG and aTc, whereas the mRNA (SRRR:sfGFP) is constitutively expressed from promoter J23119. The two sRNAs first interact to form a complex that is then able to activate a *cis*-repressed gene. The reporter gene encodes a sfGFP. (B) Fluorescence results (arbitrary units, AU) from the sRNA systems trigR31, trigR32, trigR1, trigR2 and trigR11 for all possible combinations of inducers. Error bars represent standard deviations over three biological replicates. The structural schemes of each single species implementing a system are shown. In each case, the asterisk (or two asterisks in brackets) denotes $P < 0.05$, one-tailed Welch *t*-test, comparing the fluorescence level when both inducers are present with respect to the level when there is only one inducer (or the level reached by the additive effect of the two inducers).

found significant activation of sfGFP in the presence of both IPTG and aTc only for cognate pairs (one-tailed Welch *t*-test, $P < 0.05$; Figure 4C and F). These results suggest that different RNA hybridization networks can be deployed in the same cell.

Characterization of RNA hybridization networks at the single-cell level

We then decided to study the dynamic behavior of our computational designs in single *E. coli* cells, as this would reveal to what extent the response is homogeneous (5,6,10). Flow cytometry experiments revealed significant bacterial population shift in response to both inducers (Mann–Whitney *U*-test, $P < 0.05$; Figure 5A; results for systems trigR31, trigR11 and trigR2). The reported dynamic ranges at the single-cell level are similar to those measured for the whole population (Supplementary Figure S11A). These results showed that each individual cell responds to the inducers in a relatively homogeneous manner (unimodal distributions). The observed cell-to-cell variability in output protein expression is comparable to previous scenarios of simple riboregulation in the cases of trigR31 and trigR2 (5,6,10), but system trigR11 presents larger spread (Supplementary Figure S11B).

To further explore the cell-to-cell variability during the induction dynamics of the systems, we performed a time-dependent characterization of system trigR2 using microfluidic lab-on-chip devices (Supplementary Figure S4) (3,40). This allowed us to monitor sfGFP expression in individual cells stimulated with a varying concentration of both inducers (Figure 5B). A square wave of IPTG and aTc with a period of 8 h was applied (i.e. 4 h induction/ON and 4 h relaxation/OFF), which stimulated increases and decreases of fluorescence in response (three pulses are shown in Figure 5B). We observed a delay of 25 min in the rise of fluorescence with respect to the rise of the inducers, probably due to the time required to accumulate enough RNAs. In addition, we observed certain homogenization in gene expression levels over time, as the level of noise (here, cell-to-cell variability) was much higher in the first pulse (coefficient of variation at maximal expression, CV = 21%) than in the third pulse (CV = 8%). This might be the consequence of tracking different lineages, as the number of tracked cells increases with time and variability is lower among cells of the same lineage (46). Overall, these results also confirmed the

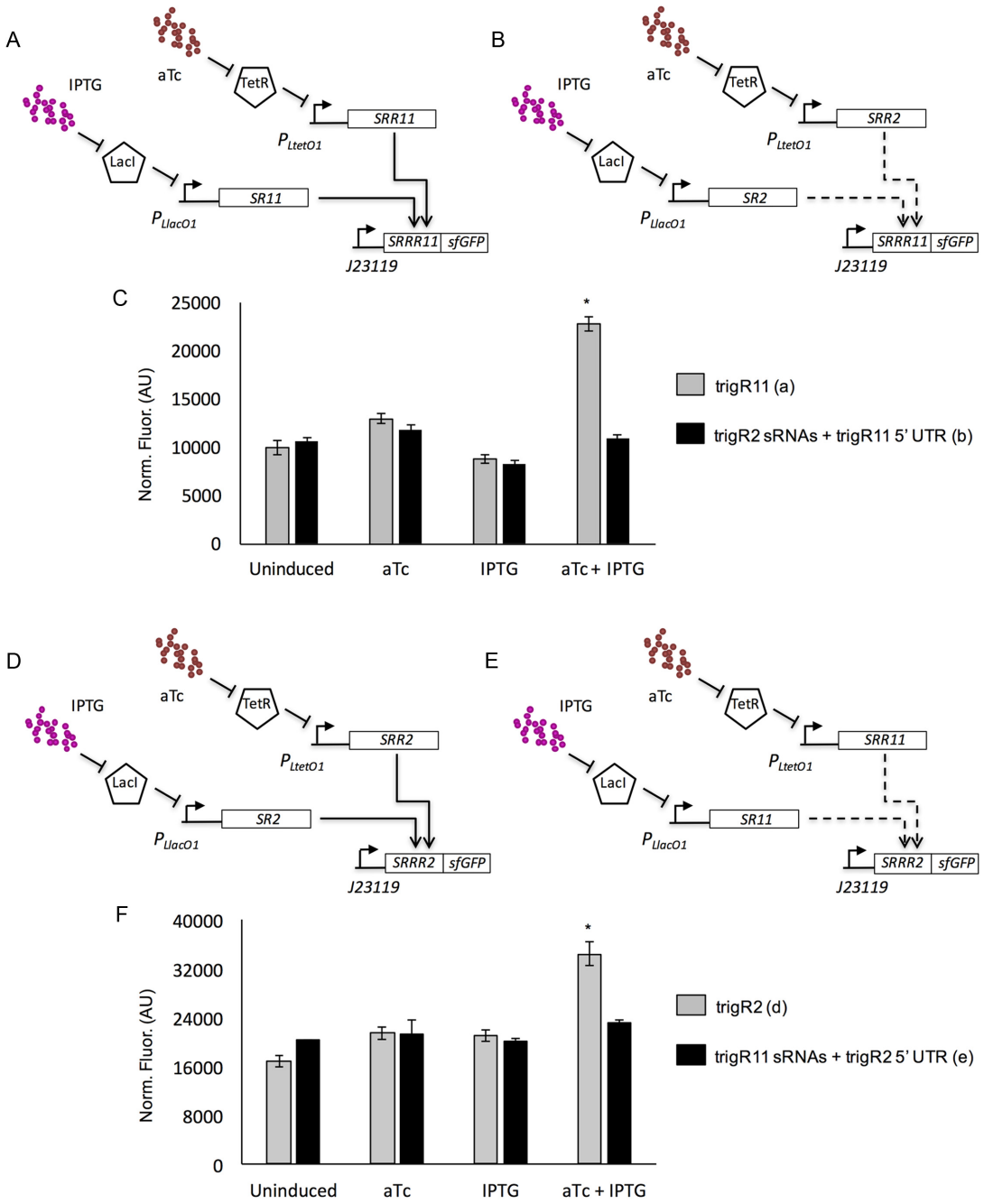

Figure 4. Characterization of the orthogonality of two designer RNA hybridization networks (trigR11 and trigR2) in bacterial cell populations. (**A**) Scheme of the system trigR11 (with cognate sRNAs and 5′ UTR). (**B**) Scheme of a crossed system with non-cognate elements, where the sRNAs correspond to system trigR2 and the 5′ UTR corresponds to system trigR11. Promoters P_{LlacO1} and P_{LtetO1} control the expression of the two sRNAs (SR and SRR), which can be tuned with external inducers IPTG and aTc, whereas the mRNA (SRRR:sfGFP) is constitutively expressed from promoter J23119. (**C**) Fluorescence results (arbitrary units, AU) from the systems shown in (A) and (B). Error bars represent standard deviations over three biological replicates. (**D**) Scheme of the system trigR2 (with cognate sRNAs and 5′ UTR). (**E**) Scheme of a crossed system with non-cognate elements, where the sRNAs correspond to system trigR11 and the 5′ UTR corresponds to system trigR2. (**F**) Fluorescence results (arbitrary units, AU) from the systems shown in (D) and (E). Three biological replicates. In both cases, the asterisk denotes $P < 0.05$, one-tailed Welch *t*-test, comparing the fluorescence level for the cognate pair with respect to the level for the non-cognate pair.

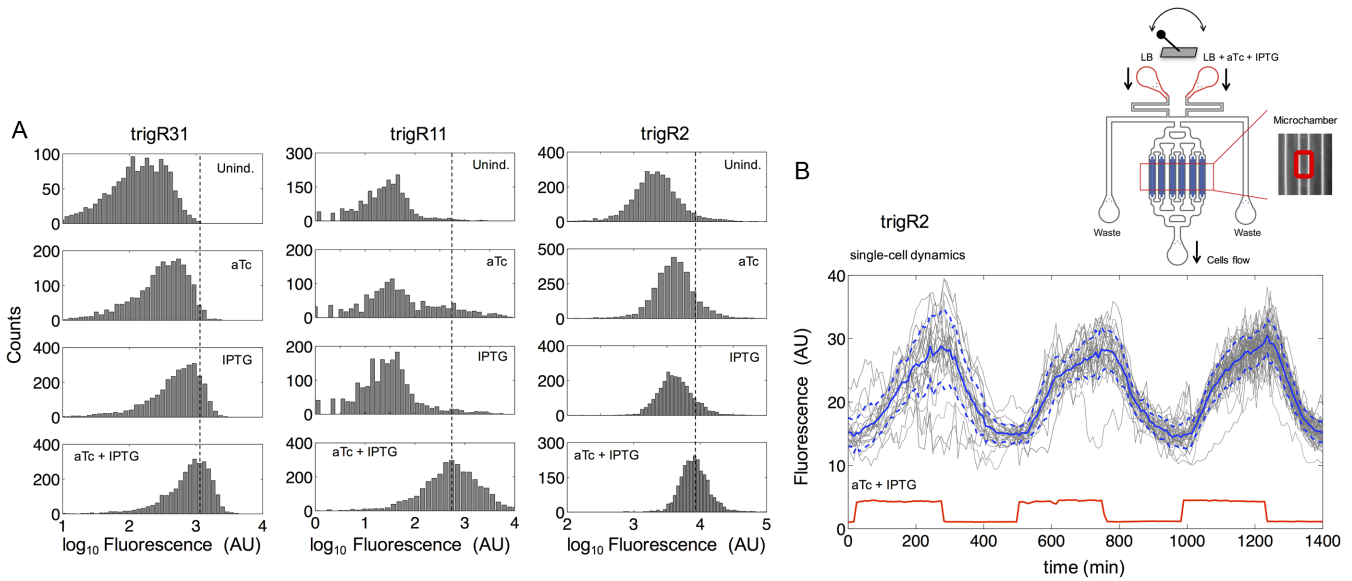

Figure 5. Functional characterization of designer RNA hybridization networks in single bacterial cells. (**A**) Fluorescence distributions of multiple individual cells obtained by flow cytometry for systems trigR31, trigR11 and trigR2. Unind., uninduced. (**B**) Dynamic single-cell tracking of fluorescence (arbitrary units, AU) in one microchamber of the microfluidics device under time-dependent induction with IPTG and aTc for system trigR2 (~100 cells). Both inducers were applied with a period of 8 h (i.e. 4 h induction/ON and 4 h relaxation/OFF; square wave). The solid and dashed lines (in blue) correspond to the mean and plus/minus the standard deviation for the entire cell population, respectively. Sulforhodamine B (red fluorescent dye) was used to monitor the inducer time-dependent profile (in red). A scheme of the device is shown at the top of the panel. Bacterial cells are trapped in the microchambers (zoomed in) and exposed to a continuous flow of media, either LB or LB with inducers (switching controlled with pumps).

homogeneous behavior, and that the system, as expected, is reversible *in vivo*.

Molecular characterization of RNA hybridization networks

To gain mechanistic insight into the hybridizations that define the networks, we characterized the different RNA-RNA interactions by native polyacrylamide gel electrophoresis (PAGE) (38). We chose to analyze the systems trigR2, trigR31 and trigR11, as they represent three different design types. The complementary DNAs corresponding to the RNA species were first transcribed *in vitro* (for the sRNA species without transcription terminators), and then purified and quantified. We mixed the three individual species (SRRR, SRR and SR), and all combinations of two of these species. These mixtures, along with the individual RNAs as controls, were loaded on polyacrylamide gels and separated electrophoretically. The same amount of each RNA per lane was used. For systems trigR2 (Figure 6A; see also Supplementary Figure S12A) and trigR31 (Figure 6C; see also Supplementary Figure S12B), native PAGE analyses revealed the intermolecular interactions between SR and SRR, and between the resulting sRNA complex (SRR*) and SRRR (Figure 6B and D, lanes 6 and 7). Additionally, they revealed a marginal intermolecular interaction between SRR (in the OFF state) and SRRR in trigR2 and trigR31 (Figure 6B and D, lane 4), and also between SR and SRRR in trigR31 (Figure 6D, lane 5). These undesired interactions could be explained, at least in part, by the corresponding free energies of hybridization, which may indeed favor the formation of those complexes (Supplementary Table S3). The electrophoretic analyses also confirmed the intermolecular interactions between SR and SRR, and between SRR* and SRRR for system trigR11 (Supplementary Figure S13).

We also quantified the different species in the electrophoresis gels (39) by considering band intensity proportional to mass. When SR and SRR reacted, we obtained a global mass fraction (mass of SRR* out of the total mass) of 42% in the case of system trigR2, 62% in the case of trigR31, and 21% in the case of trigR11. We also calculated an apparent dissociation constant (by translating the mass fractions into molar fractions; see details in Supplementary Information) for the interaction between SR and SRR of 65 μM for trigR2, 31 μM for trigR31, and 247 μM for trigR11. In addition, when SR, SRR and SRRR reacted, we obtained a global mass fraction (SRRR* over total) of 29% in the case of system trigR2, 28% in the case of trigR31, and 19% in the case of trigR11. We also calculated an apparent dissociation constant for the interaction between SRR* and SRRR of 33 μM for trigR2, 110 μM for trigR31, and 55 μM for trigR11. Taken together, these results show that synthetic RNAs need to be highly expressed to ensure hybridization (47).

Energetic and structural predictions compared to experimental data

To validate the thermodynamic model, we balanced the computational and experimental results. Supplementary Table S3 shows the free energies that characterize the systems, as predicted by Vienna RNA (26) (see in Supplementary Information how to develop the general objective function expounded in Figure 1B). Subsequently, we quantified, according to our native PAGE analyses (Figure 6 and Supplementary Figure S13), the apparent dissociation constant

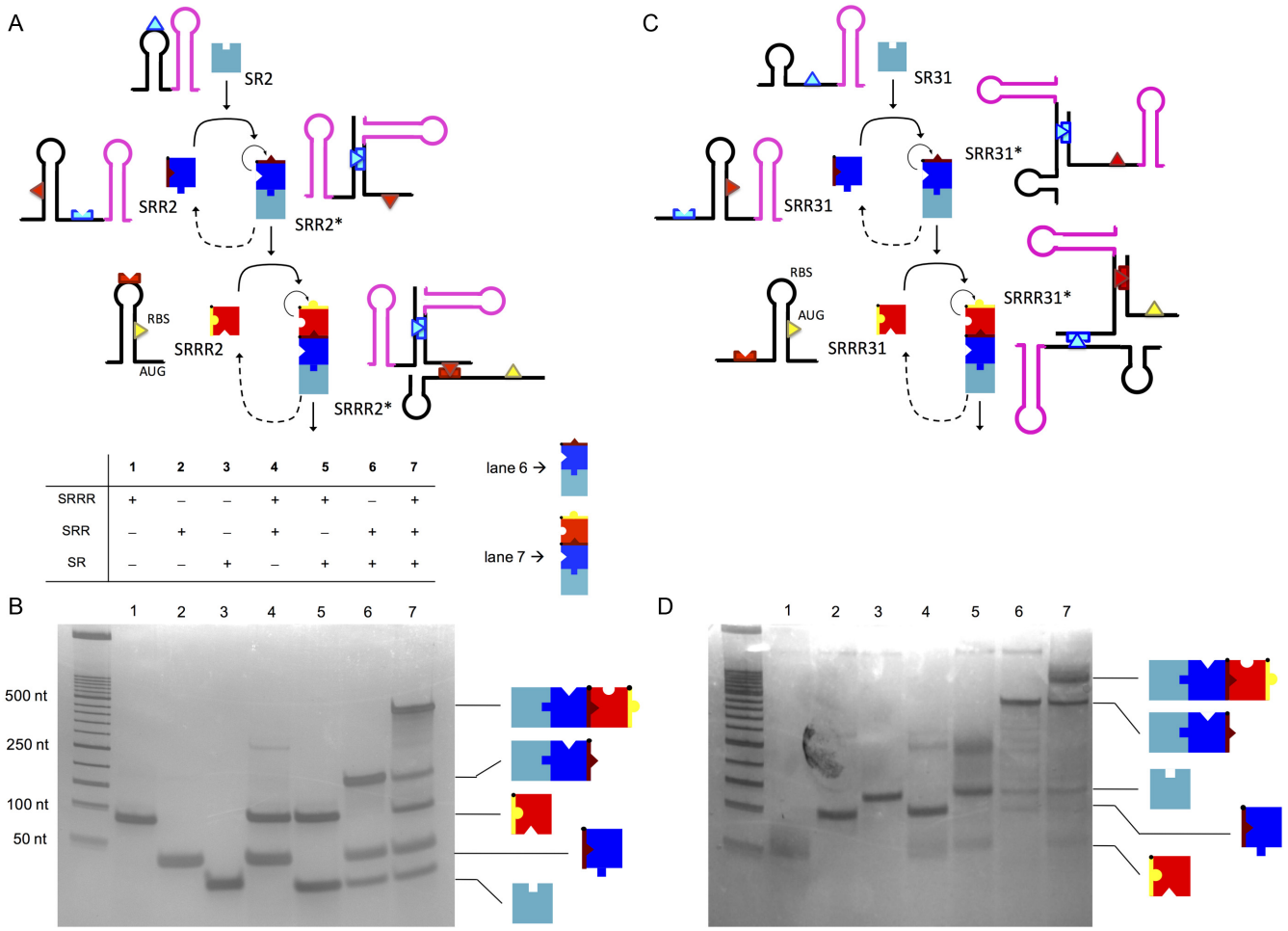

Figure 6. Molecular characterization of designer RNA hybridization networks *in vitro*. (**A**, **C**) Structures of the species implementing the systems trigR2 and trigR31. The toehold for the interaction between the two sRNAs is shown in light blue. The toehold for the interaction between the heterodimer (sRNA complex) and the 5′ UTR is shown in red. In the 5′ UTR SRRR2 the RBS works as the downstream control element, while in SRRR31 the start codon AUG does (both shown in yellow). The transcription terminator T500 was used in SRR2 and SRR31, while the terminator TrrnC was used in SR2 and SR31. (**B**, **D**) Electrophoretic analysis showing the hierarchical interaction between sRNAs. The formation of the heterodimer and heterotrimer is shown in lanes 6 and 7, respectively.

for each potential interaction, i.e. between SR and SRR (lane 6 in Figure 6B), SR and SRRR (lane 5), SRR and SRRR (lane 4), and SRR* and SRRR (lane 7). We obtained twelve different values for systems trigR2, trigR11 and trigR31, which we compared with the corresponding free energies of hybridization. In this case, the free energy of activation does not matter, because the RNAs were first denatured at 95°C and then cooled to room temperature (38). We found a significant correlation between the experimental constants (in log scale) and the predicted energies (Pearson correlation, $r = 0.758$, $P = 0.004$; Figure 7A), suggesting that the interactions among RNAs are well captured by the model.

In addition, we quantified the activation fold for each induced state (i.e., aTc, IPTG or both) relative to the uninduced state, according to our fluorescence data (Figure 3B). The expression level depends on the degree of de-repression of the 5′ UTR of the mRNA. For each induced state, we defined an objective free energy accounting for that de-repression, which we assessed with the different fold values. In the case of induction with just aTc (or IPTG), it was the sum of the free energies of hybridization and activation between SRR (or SR) and SRRR, as well as the free energy required to de-repress the 5′ UTR in the resulting complex (25). In the case of both inducers, it was the sum of the free energies of hybridization and activation between SRR* and SRRR (having neglected the potential effect of SR and SRR), as well as the free energy required to de-repress the 5′ UTR in SRRR*. Again, we found a significant correlation between the experimental activation folds (in log scale) and the predicted energies (Pearson correlation, $r = –0.735$, $P = 0.002$; Figure 7B), suggesting that our objective function is a well predictor of riboregulatory activity.

Finally, the higher basal expression in the case of trigR31 and trigR32 (i.e., activation with either aTc or IPTG alone) could be explained, at least in part, by the more negative free energies of hybridization between SR or SRR and SRRR. These systems also present larger toehold sequences. However, the contribution of the free energy of toehold hybridization to the reaction kinetics becomes saturated (48),

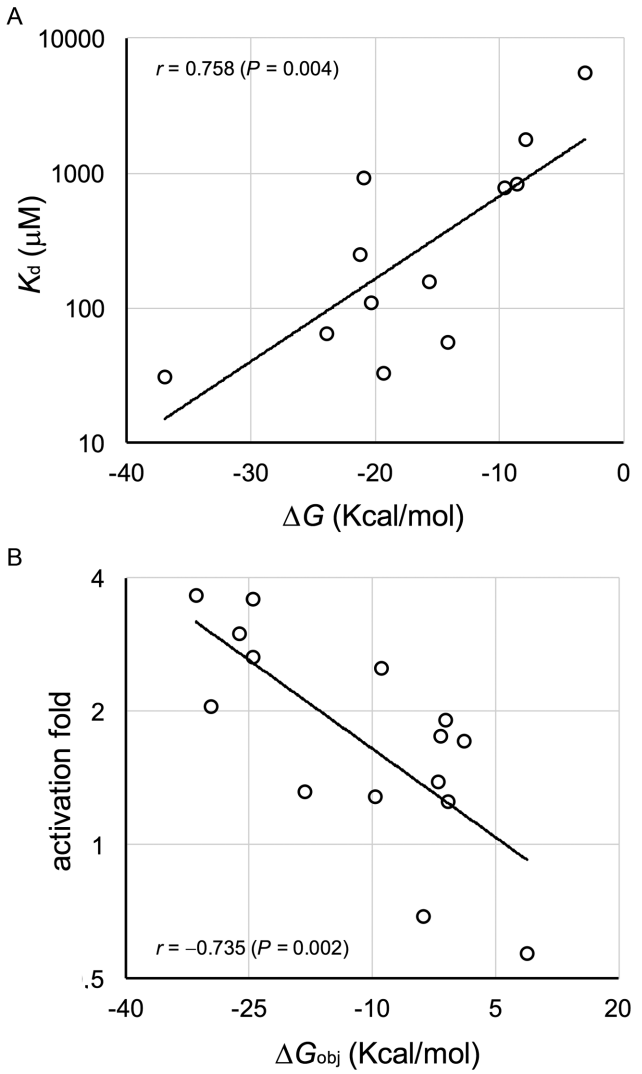

Figure 7. Predicted free energies versus activity of designer RNA hybridization networks. (**A**) Linear correlation between the apparent dissociation constant (in log scale) and the free energy of hybridization. The data shown are for systems trigR2, trigR11 and trigR31, considering the potential interactions between SR and SRR, SR and SRRR, SRR and SRRR, and SRR* and SRRR. Two-tailed Student *t*-based correlation test, $P < 0.05$. (**B**) Linear correlation between the activation fold (in log scale, relative to the uninduced state) and the objective energy of hybridization. The data shown are for all systems, considering the fluorescence increase due to aTc, IPTG and finally aTc and IPTG. Two-tailed Student *t*-based correlation test, $P < 0.05$.

which is in agreement with the similar dynamic range displayed by all engineered systems.

Extension of the engineered RNA hybridization networks

Larger networks could be engineered provided they do not impose a serious cost for the host cell (here, *E. coli*) (13). The cost can be produced either because the networks consume excessive resources for expression, or because the sRNAs interfere with endogenous mRNAs. Supplementary Table S4 shows the cell growth rates upon expression of our engineered RNA systems in each induction condition, revealing a moderate system-dependent cost. In particular, trigR11 is the costliest system, reducing growth in at most 35%, while trigR1 is the less costly system (the one with the lowest sfGFP expression), with no apparent growth reduction. These data suggest that heterologous protein expression is more determinant of growth reduction than heterologous sRNA expression. Supplementary Table S5 shows potential off-target effects, despite our sequences are fully synthetic, but with no apparent consequence on cell physiology.

For illustrative purposes, we reshaped the network architecture of system trigR31 by incorporating a new RNA species (Supplementary Figure S14) (49). In addition, Supplementary Figure S15 exemplifies, from a theoretical point of view, the ability of RNA hybridization networks to build a computing machine (a simplified case of a Turing machine (50); sequences provided in Supplementary Table S6, based on trigR31 and trigR32; see also Supplementary Figure S16). These extensions are however limited by the dependence on the genetic background of the performance of systems trigR31 and trigR32 (see details in Supplementary Information).

DISCUSSION

Here, we conceived a general framework for the computational design of RNA hybridization networks to function in living cells (Figure 1). This allows the design of structured RNA molecules with multiple interaction domains, whose activities are conditional to the binding with other molecules, thus resulting in a network of RNA hybridizations. These RNA molecules are hence elements offering novel possibilities for engineering functional, synthetic gene circuits (Supplementary Figure S14), and they add to an increasing toolbox of regulatory RNAs to control gene expression in *trans* and in a combinatorial manner (6,8). We exemplified this by designing different RNA hybridization chain reactions. Designer systems were verified for activity by characterizing the different dynamic ranges with a reporter protein at the population and single-cell levels (Figures 3 and 5), as well as by capturing all possible molecular interactions with native PAGE (Figure 6 and Supplementary Figure S13).

The computational design was possible as nucleic acids are molecules with much higher interaction programmability than proteins (5–8). A thermodynamic model allowed assessing the performance of the different RNA sequences. This way, the sequences implementing the resulting networks (Supplementary Figure S6, Table S1), defined by a set of desired on-target complexes and a set of undesired off-target complexes, satisfy all energetic and structural objectives (Supplementary Figures S1 and S5, Table S3). Here, we used Vienna RNA (26), but other RNA calculators (28,29) could also have been used. Moreover, some of these sequences were designed *de novo* by following a heuristic optimization algorithm (Monte Carlo simulated annealing; Supplementary Figure S2) (5), but other sequences were designed rationally (Supplementary Figure S6f). The *de novo* sequence design could also have been approached by dynamic programming with NUPACK (28,51), as previously done (6).

Nevertheless, the moderate activation fold of our RNA devices might not be adequate for some applications, even though cellular behavior can be reprogrammed (e.g. apoptosis control in eukaryotic cells) with small dynamic ranges (52). Moreover, the correct action of the RNAs might be, in certain cases, modulated by endogenous factors not considered in the design, leading to functional failures of the networks or excessive impact on the physiology of the cell.

Finally, RNA hybridization networks might be very useful to perform bio-logical computations in living cells, due to their ability for storing and retrieving information (e.g. Supplementary Figure S15 shows such ability with the prototype of a computing machine). Future work should be focused on refining and validating experimentally this type of molecular machines and on their exploitation in applied scenarios (53). In addition, RNA hybridization networks might be adapted to organisms other than *E. coli* (including eukaryotic hosts), as they are mainly based on physical interactions. This should be accomplished by only redesigning the interface with the output-protein expression machinery. Certainly, as our ability to design multifaceted RNAs increases, more complex bio-logical computing systems are expected to be developed.

SUPPLEMENTARY DATA

Supplementary Data are available at NAR Online.

ACKNOWLEDGEMENTS

We thank V. Singh and T. Cordero for help in the lab, and M. Kushwaha for useful comments.
Author contributions: G.R. and A.J. conceived this study. G.R., J.A.D. and A.J. designed the experiments. G.R., S.P., S.S. and E.M. performed the experiments. G.R., S.P., S.S., J.A.D. and A.J. analyzed the data. G.R. and A.J. wrote the manuscript with input of J.A.D.

FUNDING

The Consejo Superior de Investigaciones Científicas (CSIC) Intramural [grant number 201440I017]; the Ministerio de Economía, Industria y Competitividad (MINECO)/FEDER [grant number BFU2015–66894-P]; and the AXA Research Fund Postdoctoral fellowship to G.R. The predoctoral fellowship [grant number AP2012-3751, MECD] to E.M. The Ministerio de Economía, Industria y Competitividad (MINECO) [grant numbers BIO2014-54269-R, AGL2013-49919-EXP] to J.A.D. The 7th Framework Programme [grant numbers 610730 (EVO-PROG), 613745 (PROMYS)]; the Horizon 2020 Marie Sklodowska-Curie [grant number 642738 (MetaRNA)]; the Engineering and Physical Sciences Research Council (EPSRC) and the Biotechnology and Biological Sciences Research Council (BBSRC) [grant number BB/M017982/1 (WISB centre)]; and the School of Life Sciences (U. Warwick) [startup allocation] to A.J. Funding for open access charge: EPSRC/BBSRC [BB/M017982/1 to A.J.].
Conflict of interest statement. None declared.

REFERENCES

1. Ausländer,S., Ausländer,D., Müller,M., Wieland,M. and Fussenegger,M. (2012) Programmable single-cell mammalian biocomputers. *Nature*, **487**, 123–127.
2. Friedland,A.E., Lu,T.K., Wang,X., Shi,D., Church,G. and Collins,J.J. (2009) Synthetic gene networks that count. *Science*, **324**, 1199–1202.
3. Danino,T., Mondragon-Palomino,O., Tsimring,L. and Hasty,J. (2010) A synchronized quorum of genetic clocks. *Nature*, **426**, 326–330.
4. Nielsen,A.A.K., Der,B.S., Shin,J., Vaidyanathan,P., Paralanov,V., Strychalski,E.A., Ross,D., Densmore,D. and Voigt,C.A. (2016) Genetic circuit design automation. *Science*, **352**, aac7341.
5. Rodrigo,G., Landrain,T.E. and Jaramillo,A. (2012) De novo automated design of small RNA circuits for engineering synthetic riboregulation in living cells. *Proc. Natl. Acad. Sci. U.S.A.*, **109**, 15271–15276.
6. Green,A.A., Silver,P.A., Collins,J.J. and Yin,P. (2014) Toehold switches: de-novo-designed regulators of gene expression. *Cell*, **159**, 925–939.
7. Dirks,R.M. and Pierce,N.A. (2004) Triggered amplification by hybridization chain reaction. *Proc. Natl. Acad. Sci. U.S.A.*, **101**, 15275–15278.
8. Chappell,J., Takahashi,M.K. and Lucks,J.B. (2015) Creating small transcription activating RNAs. *Nat. Chem. Biol.*, **11**, 214–220.
9. Takahashi,M.K., Chappell,J., Hayes,C.A. *et al.* (2014) Rapidly characterizing the fast dynamics of RNA genetic circuitry with cell-free transcription-translation (TX-TL) systems. *ACS Synth. Biol.*, **4**, 503–515.
10. Isaacs,F.J., Dwyer,D.J., Ding,C., Pervouchine,D.D., Cantor,C.R. and Collins,J.J. (2004) Engineered riboregulators enable post-transcriptional control of gene expression. *Nat. Biotechnol.*, **22**, 841–847.
11. Bayer,T.S. and Smolke,C.D. (2005) Programmable ligand-controlled riboregulators of eukaryotic gene expression. *Nat. Biotechnol.*, **23**, 337–343.
12. Lucks,J.B., Qi,L., Mutalik,V.K., Wang,D. and Arkin,A.P. (2011) Versatile RNA-sensing transcriptional regulators for engineering genetic networks. *Proc. Natl. Acad. Sci. U.S.A.*, **108**, 8617–8622.
13. Na,D., Yoo,S.M., Chung,H., Park,H., Park,J.H. and Lee,S.Y. (2013) Metabolic engineering of Escherichia coli using synthetic small regulatory RNAs. *Nat. Biotechnol.*, **31**, 170–174.
14. Liu,C.C., Qi,L., Lucks,J.B., Segall-Shapiro,T.H., Wang,D., Mutalik,V.K. and Arkin,A.P. (2012) An adaptor from translational to transcriptional control enables predictable assembly of complex regulation. *Nat. Methods*, **9**, 1088–1094.
15. Qi,L.S., Lucks,J.B., Liu,C.C., Mutalik,V.K. and Arkin,A.P. (2012) Engineering naturally occurring trans-acting non-coding RNAs to sense molecular signals. *Nucleic Acids Res.*, **40**, 5775–5786.
16. Desai,S.K. and Gallivan,J.P. (2004) Genetic screens and selections for small molecules based on a synthetic riboswitch that activates protein translation. *J. Am. Chem. Soc.*, **126**, 13247–13254.
17. Weigand,J.E., Sanchez,M., Gunnesch,E.B., Zeiher,S., Schroeder,R. and Suess,B. (2008) Screening for engineered neomycin riboswitches that control translation initiation. *RNA*, **14**, 89–97.
18. Wachsmuth,M., Findeiß,S., Weissheimer,N., Stadler,P.F. and Mörl,M. (2013) De novo design of a synthetic riboswitch that regulates transcription termination. *Nucleic Acids Res.*, **41**, 2541–2551.
19. Wieland,M. and Hartig,J.S. (2008) An improved aptazyme design and in vivo screening enable riboswitching in bacteria. *Angew. Chem. Int. Ed.*, **47**, 2604–2607.
20. Carothers,J.M., Goler,J.A., Juminaga,D. and Keasling,J.D. (2011) Model-driven engineering of RNA devices to quantitatively program gene expression. *Science*, **334**, 1716–1719.
21. Klauser,B. and Hartig,J.S. (2013) An engineered small RNA-mediated genetic switch based on a ribozyme expression platform. *Nucleic Acids Res.*, **41**, 5542–5552.
22. Shen,S., Rodrigo,G., Prakash,S., Majer,E., Landrain,T.E., Kirov,B., Daros,J.A. and Jaramillo,A. (2015) Dynamic signal processing by ribozyme-mediated RNA circuits to control gene expression. *Nucleic Acids Res.*, **43**, 5158–5170.
23. Sternberg,J.B. and Pierce,N.A. (2014) Exquisite sequence selectivity with small conditional RNAs. *Nano Lett.*, **14**, 4568–4572.

24. Hochrein,L.M., Schwarzkopf,M., Shahgholi,M., Yin,P. and Pierce,N.A. (2013) Conditional Dicer substrate formation via shape and sequence transduction with small conditional RNAs. *J. Am. Chem. Soc.*, **135**, 17322–17330.
25. Rodrigo,G., Landrain,T.E., Majer,E., Daròs,J.-A. and Jaramillo,A. (2013) Full design automation of multi-state RNA devices to program gene expression using energy-based optimization. *PLoS Comput. Biol.*, **9**, e1003172.
26. Hofacker,I.L., Fontana,W., Stadler,P.F., Bonhoeffer,L.S., Tacker,M. and Schuster,P. (1994) Fast folding and comparison of RNA secondary structures. *Monatsh. Chem.*, **125**, 167–188.
27. Mathews,D.H., Disney,M.D., Childs,J.L., Schroeder,S.J., Zuker,M. and Turner,D.H. (2004) Incorporating chemical modification constraints into a dynamic programming algorithm for prediction of RNA secondary structure. *Proc. Natl. Acad. Sci. U.S.A.*, **101**, 7287–7292.
28. Dirks,R.M., Bois,J.S., Schaeffer,J.M., Winfree,E. and Pierce,N.A. (2007) Thermodynamic analysis of interacting nucleic acid strands. *SIAM Rev.*, **49**, 65–88.
29. Wright,P.R., Georg,J., Mann,M., Sorescu,D.A., Richter,A.S., Lott,S., Kleinkauf,R., Hess,W.R. and Backofen,R. (2014) CopraRNA and IntaRNA: predicting small RNA targets, networks and interaction domains. *Nucleic Acids Res.*, **42**, W119–W123.
30. Adleman,L.M. (1994) Molecular computation of solutions to combinatorial problems. *Science*, **266**, 1021–1024.
31. Seelig,G., Soloveichik,D., Zhang,D.Y. and Winfree,E. (2006) Enzyme-free nucleic acid logic circuits. *Science*, **314**, 1585–1588.
32. Yin,P., Choi,H.M.T., Calvert,C.R. and Pierce,N.A. (2008) Programming biomolecular self-assembly pathways. *Nature*, **451**, 318–322.
33. Kirkpatrick,S., Gelatt,C.D. and Vecchi,M.P. (1983) Optimization by simulated annealing. *Science*, **220**, 671–680.
34. Pédelacq,J.-D., Cabantous,S., Tran,T., Terwilliger,T.C. and Waldo,G.S. (2003) Engineering and characterization of a superfolder green fluorescent protein. *Nat. Biotechnol.*, **24**, 79–88.
35. Hersch,G.L., Baker,T.A. and Sauer,R.T. (2004) SspB delivery of substrates for ClpXP proteolysis probed by the design of improved degradation tags. *Proc. Natl. Acad. Sci. U.S.A.*, **101**, 12136–12141.
36. Lutz,R. and Bujard,H. (1997) Independent and tight regulation of transcriptional units in Escherichia coli via the LacR/O, the TetR/O and AraC/I1-I2 regulatory elements. *Nucleic Acids Res.*, **25**, 1203–1210.
37. Sambrook,J., Fritsch,E.F. and Maniatis,T. (1989) *Molecular Cloning: A Laboratory Manual*, Cold Spring Harbor Laboratory Press, NY.
38. Shu,D., Shu,Y., Haque,F., Abdelmawla,S. and Guo,P. (2011) Thermodynamically stable RNA three-way junction for constructing multifunctional nanoparticles for delivery of therapeutics. *Nat. Nanotechnol.*, **6**, 658–667.
39. Schindelin,J., Arganda-Carreras,I., Frise,E. *et al.* (2012) Fiji: an open-source platform for biological-image analysis. *Nat. Methods*, **9**, 676–682.
40. Rodrigo,G., Kirov,B., Shen,S. and Jaramillo,A. (2013) Theoretical and experimental analysis of the forced LacI-AraC oscillator with a minimal gene regulatory model. *Chaos*, **23**, 025109.
41. Laidler,K.J. and King,M.C. (1983) The development of transition-state theory. *J. Phys. Chem.*, **87**, 2657–2664.
42. Leveau,J.H. and Lindow,S.E. (2001) Predictive and interpretive simulation of green fluorescent protein expression in reporter bacteria. *J. Bacteriol.*, **183**, 6752–6762.
43. Levine,E., Zhang,Z., Kuhlman,T. and Hwa,T. (2007) Quantitative characteristics of gene regulation by small RNA. *PLoS Biol.*, **5**, e229.
44. Sakai,Y., Abe,K., Nakashima,S., Yoshida,W., Ferri,S., Sode,K. and Ikebukuro,K. (2014) Improving the gene-regulation ability of small RNAs by scaffold engineering in Escherichia coli. *ACS Synth. Biol.*, **3**, 152–162.
45. Vogel,J. and Luisi,B.F. (2011) Hfq and its constellation of RNA. *Nat. Rev. Microbiol.*, **9**, 578–589.
46. Rodrigo,G., Bajic,D., Elola,I. and Poyatos,J.F. (2016) Antagonistic autoregulation speeds up a homogeneous response in Escherichia coli. *Sci. Rep.*, **6**, 36196.
47. Rodrigo,G., Majer,E., Prakash,S., Daros,J.A., Jaramillo,A. and Poyatos,J.F. (2015) Exploring the dynamics and mutational landscape of riboregulation with a minimal synthetic circuit in living cells. *Biophys. J.*, **109**, 1070–1076.
48. Srinivas,N., Ouldridge,T.E., Sulc,P., Schaeffer,J.M., Yurke,B., Louis,A.A., Doye,J.P.K. and Winfree,E. (2013) On the biophysics and kinetics of toehold-mediated DNA strand displacement. *Nucleic Acids Res.*, **41**, 10641–10658.
49. Mangan,S. and Alon,U. (2003) Structure and function of the feed-forward loop network motif. *Proc. Natl. Acad. Sci. U.S.A.*, **100**, 11980–11985.
50. Turing,A.M. (1936) On computable numbers, with an application to the Entscheidungsproblem. *Proc. Lond. Math. Soc.*, **42**, 230–265.
51. Wolfe,B.R. and Pierce,N.A. (2015) Sequence design for a test tube of interacting nucleic acid strands. *ACS Synth. Biol.*, **4**, 1086–1100.
52. Culler,S.J., Hoff,K.G. and Smolke,C.D. (2010) Reprogramming cellular behavior with RNA controllers responsive to endogenous proteins. *Science*, **330**, 1251–1255.
53. Benenson,Y., Paz-Elizur,T., Adar,R., Keinan,E., Livneh,Z. and Shapiro,E. (2001) Programmable and autonomous computing machine made of biomolecules. *Nature*, **414**, 430–434.

Supplementary Information

Model-based design of RNA hybridization networks implemented in living cells

Guillermo Rodrigo, Satya Prakash, Shensi Shen, Eszter Majer, José-Antonio Daròs, and Alfonso Jaramillo

It contains Supplementary Materials and Methods, Additional Texts, 16 Supplementary Figures, and 6 Supplementary Tables.

Supplementary Materials and Methods

Objectives for RNA sequence design

Our approach consisted, first, in developing an empirical thermodynamic model that allowed the computational sequence design [1, 2] and, second, in implementing genetically the designed systems to then characterize the intended behavior. To assess the performance of the RNA molecules, an objective function was calculated with a nucleotide-level energy model considering all conformational states of the system's species (SR, SRR, SRRR, all possible heterodimers, and the heterotrimer), following a combined strategy of positive and negative design. On the one hand, as positive objectives (to be minimized), we considered the free energies of activation and hybridization corresponding to the interactions between the two sRNAs and between the resulting sRNA complex and the 5' UTR. We also considered the interaction between the 5' UTR in complex with the sRNAs and the ribosome. On the other hand, as negative objectives (to be maximized), we took the free energies of activation and hybridization corresponding to the interactions between each sRNA and the 5' UTR. Also, we considered the interaction between the 5' UTR and the ribosome (see Fig. S1). This way, to design our five systems, we combined the *de novo* sequence design, by developing an iterative process of random mutations and selection according to the energy-based objective function (Fig. S2), with the rational sequence design.

Energetic and structural calculations

We used the Vienna RNA package [3] for energy and structure calculation. The calculation of the free energies of full hybridization (ΔG_1 and ΔG_2 for desired interactions, $\Delta \hat{G}_1$ and $\Delta \hat{G}_2$ for undesired ones) was done using the routine cofold. This also gives the final intermolecular structure. To calculate ΔG_2, the free energy of

hybridization between three species, we created a new sequence by simply juxtaposing the sequences of SR and SRR.

The free energies of activation cannot be directly calculated. However, we can write that they (e.g., $\Delta G_1^{\#}$) are related to the free energies of toehold hybridization given an entropic constant (*C*, i.e., $\Delta G_1^{\#} = C + \Delta G_1^{\text{toehold}}$). This way, the more negative $\Delta G_1^{\text{toehold}}$ is, the closer to 0 $\Delta G_1^{\#}$ is. Thus, the calculation of the free energies of toehold hybridization ($\Delta G_1^{\text{toehold}}$ and $\Delta G_2^{\text{toehold}}$ for desired interactions, $\Delta \hat{G}_1^{\text{toehold}}$ and $\Delta \hat{G}_2^{\text{toehold}}$ for undesired ones) was done again using the routine cofold by only considering the toehold sequences.

Finally, the calculations of the free energies that mediate the interaction between the 5' UTR (either alone or in complex with the sRNAs) and the ribosome (ΔG_3, $\Delta G_3^{\#}$, $\Delta \hat{G}_3$ and $\Delta \hat{G}_3^{\#}$) were approximated for simplicity. We considered that $\Delta G_3 + \Delta G_3^{\#}$ is related to the free energy of the *cis*-repression in SRRR*, and that $\Delta \hat{G}_3 + \Delta \hat{G}_3^{\#}$ is related to the free energy of the *cis*-repression in SRRR. This way, the stronger the *cis*-repression is, the lower translation rate is. By introducing the terms $\Delta G_{SRRR}^{\text{struct}}$ and $\Delta G_{SRRR*}^{\text{struct}}$, as done in ref. [2], we can write $\Delta G_3 + \Delta G_3^{\#} = C' + \Delta G_{SRRR*}^{\text{struct}}$ and $\Delta \hat{G}_3 + \Delta \hat{G}_3^{\#} = C'' - \Delta G_{SRRR}^{\text{struct}}$. These terms were calculated as the Hamming distance between the actual and ideal secondary structures (here, RBS paired in case of SRRR, or unpaired in case of SRRR*) and then considering an average value of 1.2 Kcal/mol per base-pair discrepancy. Note that the terms $\Delta G_{SRRR}^{\text{struct}}$ and $\Delta G_{SRRR*}^{\text{struct}}$ are positive. In addition, note that the free energies characterizing the interaction with the ribosome could also be calculated following the function proposed in ref. [4]. Further work could incorporate this to improve the accuracy of the objective function.

The resulting objective free energy to be minimized is $\sum u_{ij} (\Delta G_{ij} + \Delta G_{ij}^{\#}) =$

$\Delta G_1 + \Delta G_1^{\text{toehold}} + \Delta G_2 + \Delta G_2^{\text{toehold}} - \Delta \hat{G}_1 - \Delta \hat{G}_1^{\text{toehold}} - \Delta \hat{G}_2 - \Delta \hat{G}_2^{\text{toehold}} + \Delta G_{SRRR}^{\text{struct}}$ + $\Delta G_{SRRR*}^{\text{struct}}$. See Figs. S1 and S5 for illustrative purposes.

Notes on RNA sequence design

In case of systems trigR31 (or trigR32), element SR31 (or SR32) is directly the sRNA of system 1 (or 7) from ref. [5] [taken from plasmid pAG_TS2_AT01 (or pAG_TS2_AT07)], but using a bacterial terminator. Element SRR31 (or SRR32) is a modification of the cognate 5' UTR [plasmid pAG_TS2_KS01 (or pAG_TS2_KS07)], without linker and carrying a mutation to disrupt the RBS (GG $\rightarrow$ CC), also with a bacterial terminator. Then, a 5' UTR responsive to SRR31* (or SRR32*) was designed keeping those sRNA sequences fixed (see Table S1).

In case of system trigR11, the toehold is not hidden within the corresponding intramolecular structure (of SRR11), but it still remains inactive. This is because the hybridization free energy is not sufficient to ensure irreversible interaction (with SRRR11), and an additional species (SR11) is required for the reaction. The free energy of hybridization between SRR11* and SRRR11 is then sufficient to form the triple intermolecular folding state with a three-way junction. When constructing SRR11 and SR11, we found that both sRNAs had an active toehold that allowed them to interact. The heterodimer SRR11* has another active toehold that nucleates its binding to SRRR11 by forming a heterotrimer with the three-way junction (see Table S1 and Fig. S7).

To design the RNA elements that implement the molecular machine shown in Fig. S15, we relied on systems trigR31 and trigR32 and applied computational design to redesign the sequences. The element that work as record tape (SRtape) was derived from SR31 by adding a hairpin with the second toehold hidden. We also redesigned the

elements SRR31 and SRR32 (called SRR31bis and SRR32bis) to, on the one hand, interact with the record tape and, on the other hand, still interact with the cognate 5' UTRs (see Table S6). The elements that control the expression of the two reporter proteins in the 5' UTR are directly the elements SRRR31 and SRRR32. This way, SRtape interacts first with SRR31bis, and then with SRR32bis.

Additional plasmid construction

For systems trigR11 and trigR2, we also constructed a variant with a non-tagged sfGFP. In the construction of the control circuit where the two sRNAs are fused transcriptionally, the promoter P_{LtetO1} was used. In the construction of the circuit with two regulatory branches (Fig. S14), the element SRRb31:sfGFP was expressed from promoter J23119 (see Table S2).

Preparation for *in vitro* RNA-RNA interaction

We first constructed the cDNAs of the different RNA species of the designed system to then perform the *in vitro* transcription. We analyzed the systems trigR2, trigR11 and trigR31. We considered the sRNAs without transcription terminators and the 5' UTR until the start codon. Amplification by PCR (30 cycles, extension 0.5 min), using Phusion DNA polymerase (Thermo Scientific), was done over the template plasmid (ptrigR2, ptrigR11 or ptrigR31). The PCR products were cloned into the plasmid pUC18, where the restriction site Eco31I was previously removed. The resulting plasmids with inserts were selected by DNA cleavage with appropriate restriction enzymes. Sequences were also verified by sequencing.

In case of trigR31, element SRRR31 was not *in vitro* transcribed (presumably due to strong secondary structure), so it was digested with Esp3I to get a shorter RNA but still able to interact with the other RNAs.

For the reaction of RNA-RNA interaction, we used approximately the same amount of RNA for each of the transcripts (20 ng for systems trigR2 and trigR11, and 60 ng for system trigR31).

Apparent dissociation constant estimation

ImageJ was used to quantify the intensities of the bands [6]. We mainly focused on two lanes: the lane having the two sRNAs (species SR and SRR; to quantify the dimeric interaction), and the lane having the two sRNAs and the 5' UTR (species SR, SRR and SRRR; to quantify the trimeric interaction). With these intensities, we calculated the different mass fractions. Moreover, by knowing the RNA sequences, we translated band intensities (proportional to mass) into molar concentrations. Note that sequences could be longer in the 5' end (including GG when needed for T7 RNA polymerase) or shorter in the 3' end (excluding transcription terminators). The apparent dissociation constants were estimated by dividing the resulting molar concentrations of the reactants with respect to the products, i.e., [SR]·[SRR] / [SRR*] in case of sRNA-sRNA interaction, and [SRR*]·[SRRR] / [SRRR*] in case of (sRNA:sRNA)-5' UTR interaction.

Living cells and energy gains for fluorescence quantification

For characterization in the Infinite F500 multi-well fluorometer (TECAN), plasmids carrying all the systems (trigR31, trigR32, trigR11, trigR1 and trigR2) were transformed into DH5α-Z1 cells. The systems trigR31 and trigR32 were also

characterized in MG1655-Z1 cells, because their activity in DH5α-Z1 cells was marginal.

For systems trigR31, trigR11 and trigR1 the gain of the fluorometer was set to 35, for system trigR2 to 25 (due to strong translation rate), and for system trigR32 to 45 (due to weak translation rate). Fluorescence values were then rescaled according to the scale of gain 35.

Additional Texts

Rationale about the interaction with the ribosome

An efficient interaction between the 5' UTR of an mRNA (SRRR element) and the ribosome requires that both the RBS sequence (Shine-Dalgarno, SD) and the start codon (AUG) are within an unpaired structural context [4], i.e., not only the SD and AUG nucleotides but also the surrounding nucleotides. Thus, for an efficient *cis*-repression of translation initiation, both the RBS sequence and the start codon have to be within a paired structural context. However, this condition can be relaxed, as shown experimentally. Only the *cis*-repression of the RBS or the start codon is required to construct riboregulatory systems [1, 5]. Following these design principles, we here constructed different SRRR elements. The SRRR elements in the case of trigR1, trigR2, and trigR11 were designed by specifying the objectives of RBS occlusion in the OFF state and release in the ON state. By contrast, the SRRR elements in the case of trigR31 and trigR32 were designed by specifying the objectives of AUG occlusion and release. The resulting structure of the SRRR element in the case of trigR32 also revealed a *cis*-repression of the RBS, although it is not the system with lower expression.

Effect of the genetic background on the performance of the regulatory systems

Systems trigR31 and trigR32 were designed based on two riboregulators previously engineered and characterized [5] (see above *Notes on RNA sequence design*). In our characterizations at the population level, these systems exhibited, unexpectedly, a marginal activity in DH5α-Z1 cells. We then performed new characterizations in MG1655-Z1 cells, obtaining better results in terms of activity. Results shown in main Fig. 3 for these systems correspond to expressions in MG1655-Z1 cells. The other systems (trigR11, trigR1 and trigR2) displayed similar activities in both cell types.

Equilibrium of RNA-RNA interactions

We can assume that the underlying RNA-RNA interactions of our systems are in thermodynamic equilibrium [7]. This way, we can explain the increase in protein expression as a function of the concentrations of the RNAs. We can state that protein expression depends on the concentration of complex SRRR*. The formation of this complex in turn depends on the concentrations of SR, SRR and SRRR, as well as on the equilibrium constants of the two RNA-RNA interactions in chain.

On the one hand, the promoters P_{LlacO1} and P_{LtetO1} produce, at most, an expression level of the two sRNAs of 1-10 μM (with IPTG and aTc in the Z1 background) [8]. Moreover, the promoter J23119 may produce an expression level of the mRNA of 1 μM. Note that these expression values are estimated for a high-copy number plasmid.

On the other hand, according to our *in vitro* RNA-RNA interaction results, the effective dissociation constants are in the range of 30-300 μM. In particular, for system trigR2, we obtained K_1 = 65 μM for the SR-SRR interaction (forming the complex SRR*), and K_2 = 33 μM for the SRR*-SRRR interaction (forming the complex SRRR*). These constants depend on the free energies of hybridization and activation, as previously shown [9]. In particular, we can write $K_1 \sim \exp[\beta (\Delta G_1 + \Delta G_1^{\#})]$ and $K_2 \sim \exp[\beta (\Delta G_2 + \Delta G_2^{\#})]$, where and β is a fitting constant (see also main Fig. 7). That is, lower the free energy of hybridization (i.e., more negative), lower the dissociation constant (i.e., higher the equilibrium constant, higher affinity). And higher the free energy of activation (i.e., more positive), higher the dissociation constant (i.e., lower the equilibrium constant, lower affinity).

Because the values of the effective dissociation constants are much higher than the expected concentrations of the sRNA molecules within the cell, we can state that the system is in a linear regime. Hence, following previous calculations [9], we can write [SRR*] = [SR]·[SRR] / K_1, and [SRRR*] = [SRR*]·[SRRR] / K_2. Combining these two equations, we get [SRRR*] = [SR]·[SRR]·[SRRR] / K_1K_2, i.e., we obtain the concentration of the final complex as a product of the concentrations of the initial species. This gives a plane in log scale. Note that the expression of SRRR* could be enhanced either by mutations that modify the free energies or by increasing the concentrations of the sRNAs, both factors reshaping the equilibrium.

A model-based prediction of the formation of the complex SRRR* as a function of the concentration of the species SR and SRR, together with the experimental data of fluorescence by varying the concentrations of IPTG and aTc, is shown in Fig. S9 for system trigR2. The difference between the two surfaces may be attributed to the nonlinearity introduced in the transcription process.

Coupling of an RNA hybridization network with the cellular machinery

In vivo, sRNAs may interact with the cellular machinery to perform their functions. In *E. coli*, sRNAs often interact with the Hfq protein, which acts as a chaperone to stabilize and facilitate the binding to their targets [10]. We did not consider such interactions in our model, so we asked if we would get enhanced functionality by rationally engineering an interaction with Hfq. To this end, we created an additional system based on trigR31, which showed the less-prominent digital behavior (see main Fig. 3). We introduced an Hfq target in SRR (sequence MicF-M7.4 from ref. [11]), with the aim of increasing the interaction between SRR* and SRRR and then shifting the equilibrium towards the formation of SRRR*. But we obtained a similar result (Fig. S10a). It is

possible that fewer Hfq molecules were available in the cell compared to the expected high number of SRR molecules, and that they were hence insufficient to affect the system [10, 12] (note that the SRR was highly expressed from a plasmid, so the relative number of SRR:Hfq molecules would be low). Although more research is certainly needed, the engineering of Hfq interactions seems unlikely to increase performance in highly expressed RNA hybridization networks with optimized free energies.

Creation of a simple riboregulator from an RNA-triggered riboregulator

As we constructed an RNA-triggered riboregulator from a simple riboregulator (system trigR11; Fig. S7), we asked if the converse operation would be possible. To this end, we created a new riboregulator by transcriptionally fusing the species SR and SRR (resulting in the new species SR-SRR) from system trigR31. We then tested the new riboregulator *in vivo*, which showed a similar activation of gene expression than the original system (Fig. S10b).

Note on off-target effects

When expressing heterologous sRNAs *in vivo*, it is important to take into account that these molecules can interact by antisense mechanism with endogenous mRNAs, then producing some undesired effects on the chassis cell. Table S5 shows eventual off-target effects of some of our designed riboregulators using RNApredator [13] (considering the 5' UTRs of all mRNAs in the genome of *E. coli* K-12 MG1655), although the viability of the cell (effects on essential genes) was not compromised when expressing them (our experiments showed that bacterial cells grew normally).

Engineering combinatorial regulation with RNA-triggered riboregulators

To illustrate the ability of designing and implementing combinatorial regulatory circuits with sRNAs in living cells, we engineered a system with two regulatory branches as a proof of concept. For that, we considered our system trigR31 and took from previous work [5] the sequence of the 5' UTR (SRRb) that is responsive to the sRNA SR. We placed this *cis*-repressing element together with a sfGFP under the control of a constitutive promoter (implemented in another plasmid). This way, SR can activate sfGFP by two routes, one with an intermediate sRNA (SRR; Figs. S14a,b). Figure S14c shows the dynamic range (characterized by fluorometry) of the system, probing the interoperability of different layers of sRNAs with the allosteric toehold activation mechanism.

RNA hybridization networks for computation in living cells

To illustrate the potential applications of our engineered systems, we conceived a simplified version of a Turing machine [14] to perform computations with genetically-encoded RNAs inside a living cell, in the line of previous work *in vitro* [15, 16]. Indeed, the exploitation of RNA molecules for storage and retrieval of information *in vivo* allows the modulation of gene expression profiles according to a set of instructions processed by a machine that encodes a set of predefined rules. In our design (Fig. S15a), the machine (called Turing *head*) is implemented by RNA-triggered riboregulators, and it is able to activate predetermined gene expression programs upon reading arbitrary information linearly stored in a heterologous RNA molecule (called *tape* in the context of Turing machines). We conceived the Turing head relying on species SRR and SRRR. These RNA molecules are appropriately disposed to interact with (read) the tape, while the expression levels of different *cis*-repressed genes (A, B, etc.) register the internal state. Moreover, a multi-toehold SR molecule plays the role of the tape (the SRtape

molecule), and only one toehold (the symbol currently read) is active at a time, with an arbitrary number of hidden toeholds. The set of all possible toeholds (symbols) is the alphabet of the machine, which performs arithmetic operations according to a predefined transition state table (Fig. S15b). Upon hybridization with the cognate SRR molecule, the tape moves to the left so that the Turing head is able to read the next symbol (see Fig. S16 for an illustration of this movement for different SRtape molecules). This mechanism can be used in series to progressively read toeholds and activate genes. Of note, the intended machine registers the final state, in the form of gene expression, but does not write on the tape.

To exemplify the implementation of such a Turing machine, we here exploited the systems trigR31 and trigR32 (Fig. S15c), showing that it is possible to achieve complex computations by only relying on RNA hybridization networks. For that, we redesigned the molecules SRR31 and SRR32 (now called SRR31bis and SRR32bis, respectively). The 5' UTRs of the registry genes are directly SRRR31 and SRRR32. We also designed the new molecule SRtape to contain one toehold active and another inactive (sequences shown in Table S6). In this design, the tape has two toeholds, but it could have a larger number. This way, the Turing head reads the first active toehold through SRR31bis, triggers a regulatory cascade that activates gene A controlled by SRRR31, and the subsequent toehold in SRtape becomes active (state A in Fig. S15c).

It is interesting to make an analogy to the translation machinery [17], where the symbols in the SRtape molecule would play the role of codons and the SRR molecules the role of tRNAs.

The SRtape molecule could be introduced in the cell as DNA through horizontal gene transfer mechanisms, which would allow transferring digital information among cells. This could lead to the development of RNA-based distributed computation

platforms exploiting cell populations [18], as done with the signaling of small molecules affecting transcription factors [19].

The strategy presented here would allow the development of a read-only Turing machine, but it should be possible to use RNA to design a writing system. For that, the DNA sequence coding for the SRtape would be modified. Recombination-based methods [20] or the type IE CRISPR system [21] have been recently used to store information in DNA, illustrating that the approach could be feasible.

The cost of complex RNA-based computations

The use of RNA to implement the computations would reduce the size of the DNA piece required for encoding and would enlarge considerably the alphabet of available symbols. Indeed, a tape made of RNA of 30 instructions could be encoded in place of a single protein of average size. However, the execution of complex RNA-based programs would require the expression of a large number of molecules (sRNAs), which could impact on the cell growth rate. In particular, 10^4-10^5 molecules seem to be required for a network of two nested interactions (according to main Fig. 7a). To overcome the cost of expressing all sRNAs at a time, our RNA hybridization networks could be interfaced with RNA-guided transcriptional control mechanisms [22, 23] to turn off the unsolicited species at a given point.

Natural RNA-triggered riboregulators?

The sequences implementing our systems are fully synthetic, but appropriate bioinformatic approaches [24, 25] might unveil natural examples of RNA-triggered riboregulators. This would constitute a new layer in the host riboregulome.

Supplementary Figures

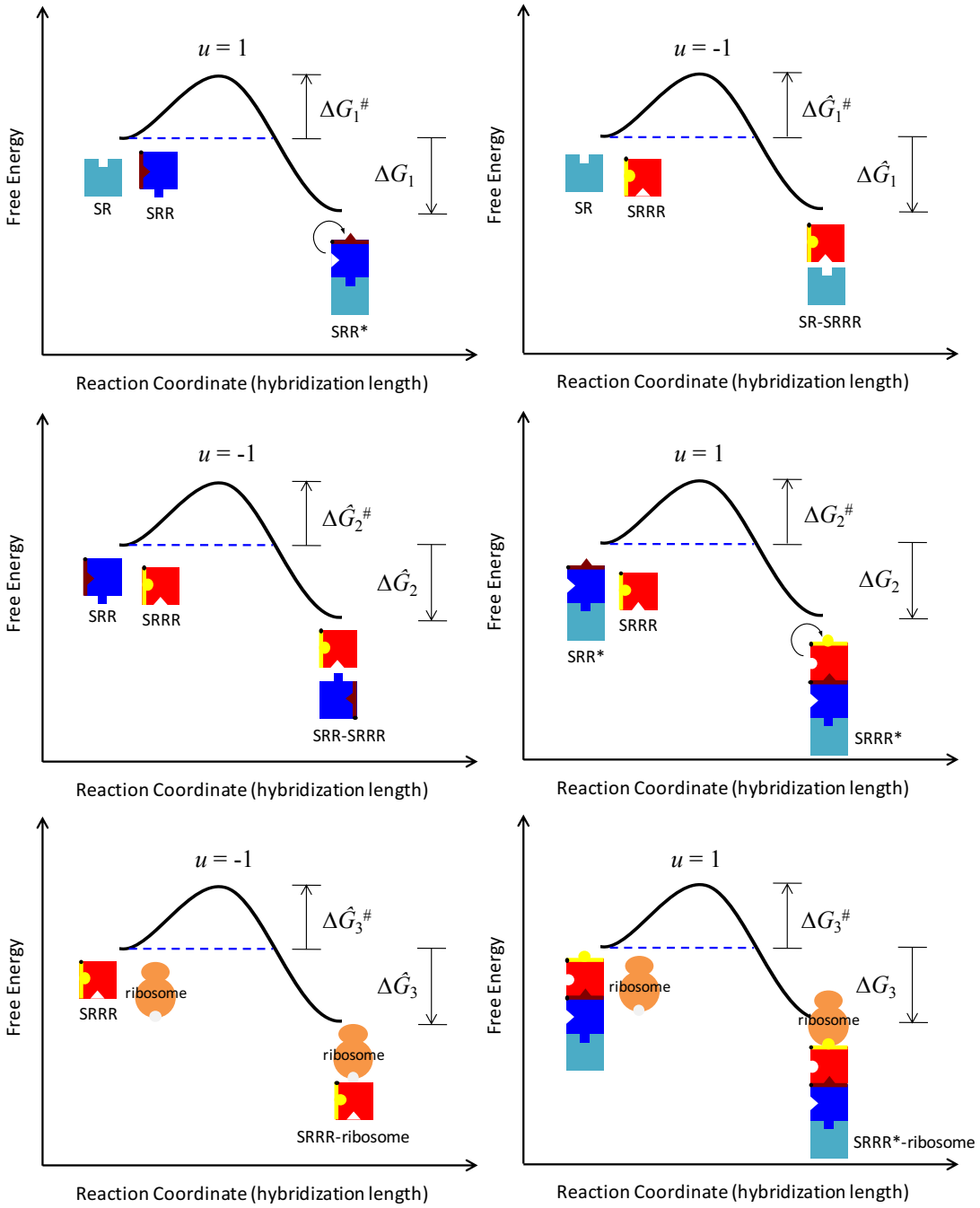

Figure S1: Illustration of all energetic terms used to design an RNA hybridization chain reaction. Here, SRRR is the expression platform (i.e., mRNA). Note that the free energy of hybridization is a negative magnitude, whereas the free energy of activation is a positive magnitude. Moreover, u indicates positive (1, energy minimization) or negative (-1, energy maximization) design. This way, the objective function to be minimized is $\Delta G_1 + \Delta G_1^{\#} - \Delta \hat{G}_1 - \Delta \hat{G}_1^{\#} + \Delta G_2 + \Delta G_2^{\#} - \Delta \hat{G}_2 - \Delta \hat{G}_2^{\#} + \Delta G_3 + \Delta G_3^{\#} - \Delta \hat{G}_3 - \Delta \hat{G}_3^{\#}$.

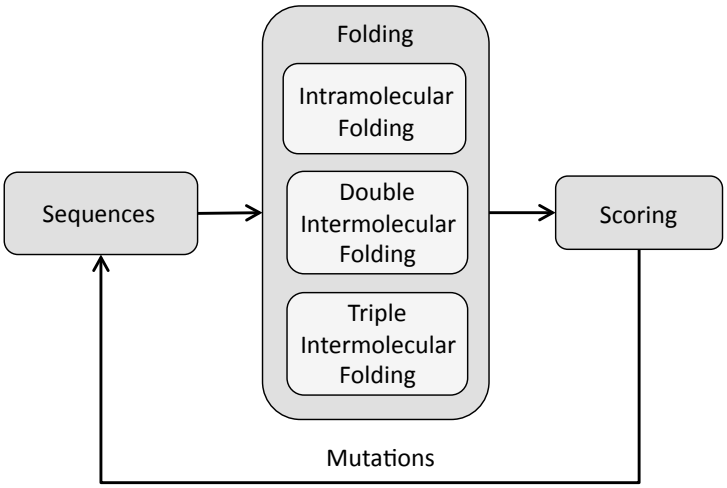

Figure S2: Scheme of the optimization loop, where three RNA sequences (SR, SRR, and SRRR) are iteratively mutated and evaluated according to the objective function. To fold the sequences, we used ViennaRNA [3].

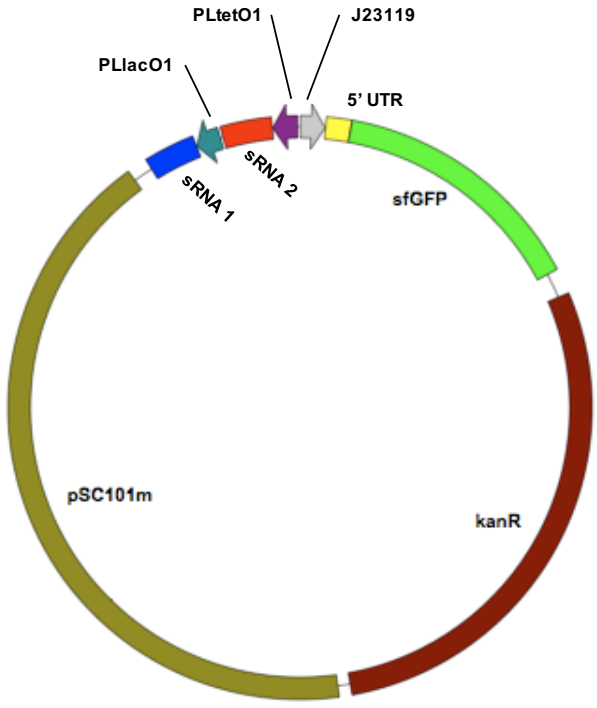

Figure S3: Map of the plasmid used in this work for expressing the designed sRNA systems. The sRNAs 1 and 2 correspond to SR and SRR, respectively, according to our terminology. The 5' UTR is named as SRRR.

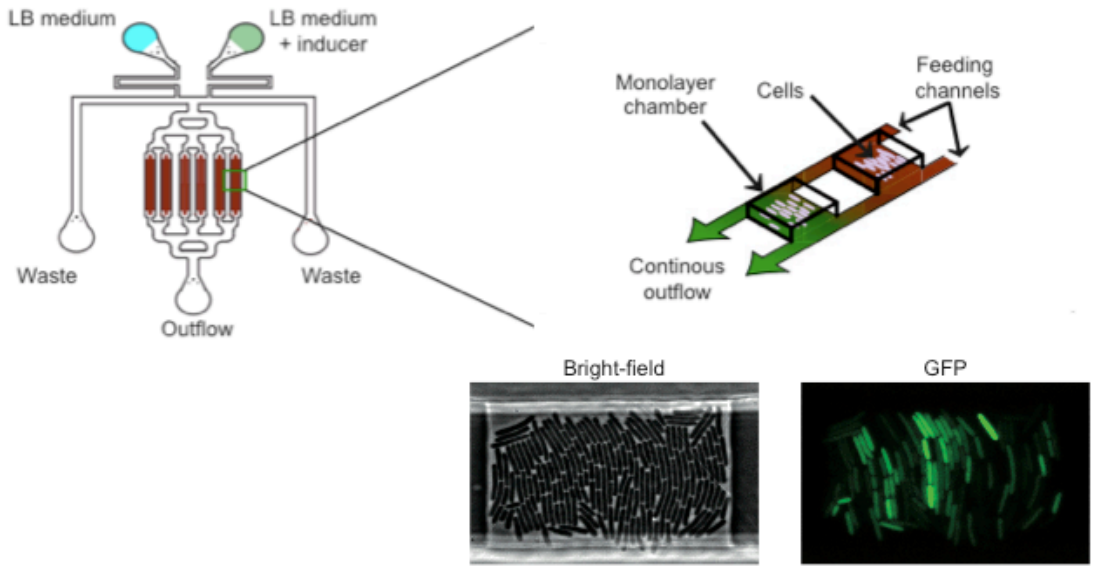

Figure S4: Scheme of the microfluidic device used to monitor GFP expression in single cells (see ref. [26] for a review of this technique). The device can receive two different input media, either LB or LB with inducers. Bacterial cells are loaded into the device and trapped in the microchambers. They are exposed to a continuous flow of media. Cell images from the bright-field channel serve for segmentation and tracking. Images from the fluorescence channel can be quantified.

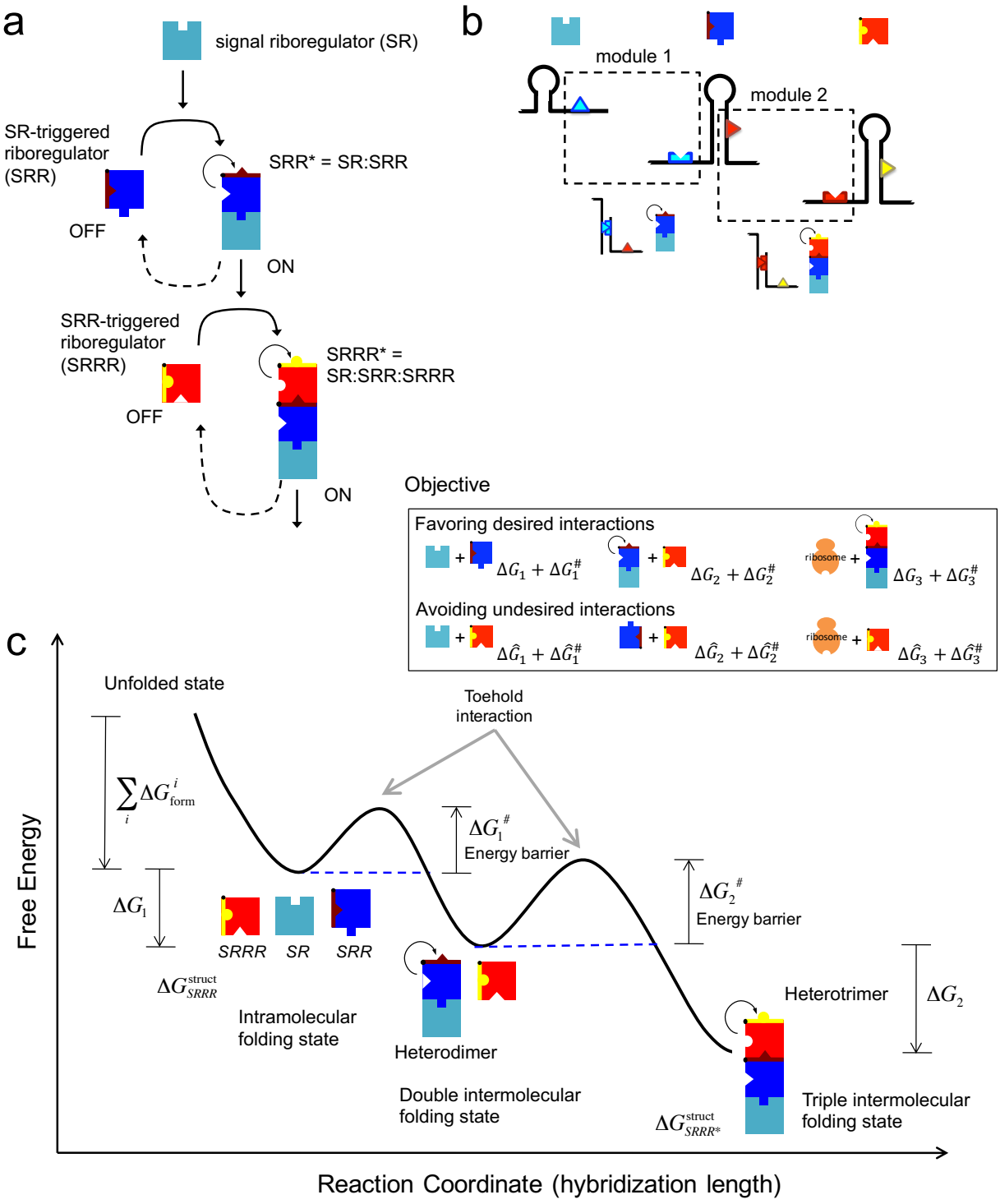

Figure S5: (a) Scheme of riboregulatory cascades implemented with RNA-triggered riboregulators (i.e., riboregulators that allosterically switch from an OFF state to an ON state upon interaction with another riboregulator). (b) Structural implementation of the cascade with allosteric programming of toehold activation. Two different interaction modules are identified. (c) Energy landscape of riboregulatory cascades (here of three molecules, named SR, SRR and SRRR). The energy landscape shows the different conformational states (intra- and intermolecular), together with the free energy terms of the objective function, as a function of a reaction coordinate (number of intermolecular base pairs). In the inset, the objective function is illustrated.

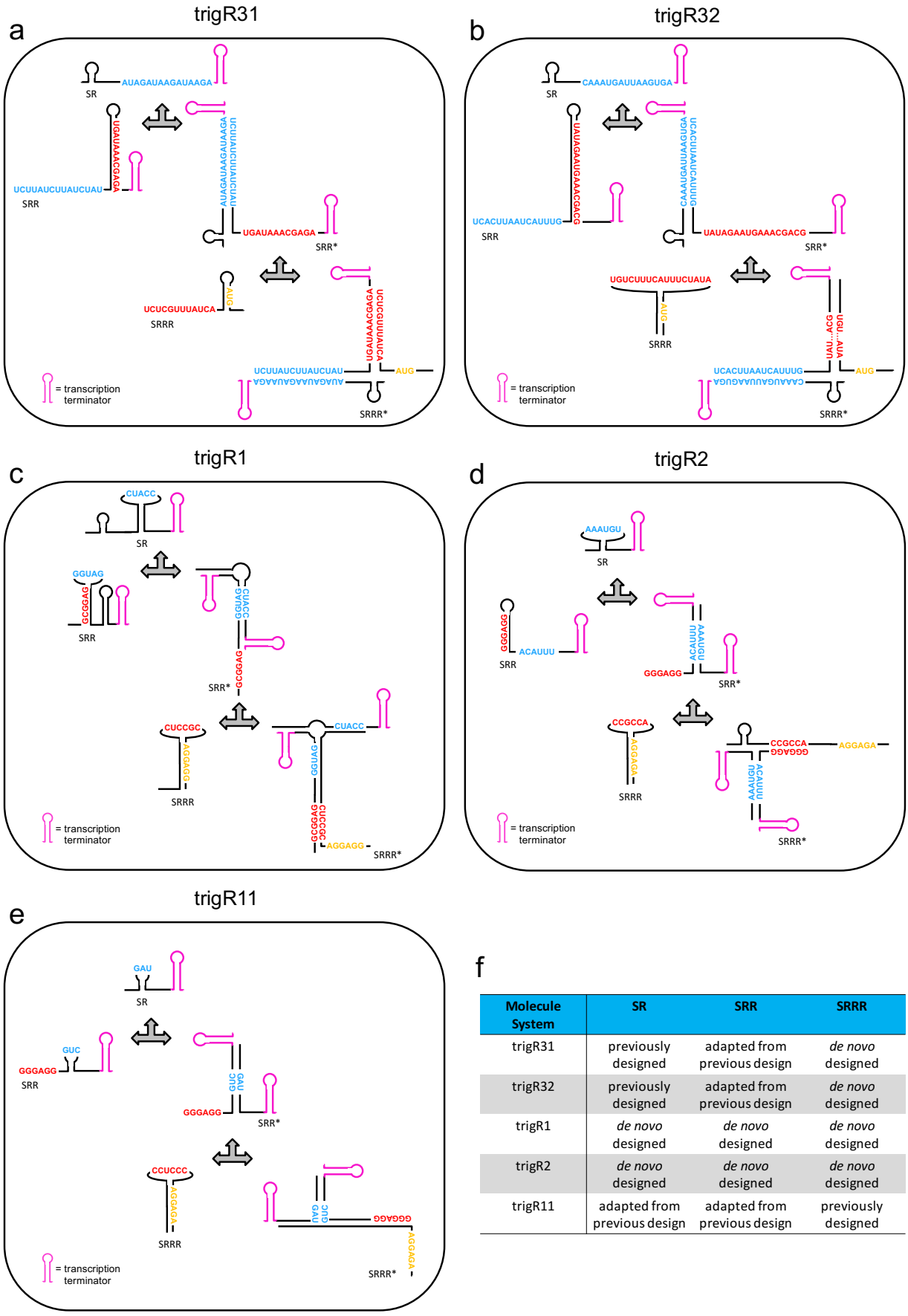

f

Molecule System	SR	SRR	SRRR
trigR31	previously designed	adapted from previous design	*de novo* designed
trigR32	previously designed	adapted from previous design	*de novo* designed
trigR1	*de novo* designed	*de novo* designed	*de novo* designed
trigR2	*de novo* designed	*de novo* designed	*de novo* designed
trigR11	adapted from previous design	adapted from previous design	previously designed

Figure S6: Sequence-structure schematics of designer RNA hybridization chain reactions: (a) trigR31, (b) trigR32, (c) trigR1, (d) trigR2, and (e) trigR11. For each system, the toehold sequence for the interaction between the two sRNAs is shown in blue, and the toehold sequence for the interaction between the heterodimer (sRNA complex) and the 5' UTR is shown in red. See Table S1 to know what transcription terminator (depicted in pink) is used in each sRNA. In the 5' UTR, the RBS or the start codon AUG (shown in yellow) works as the downstream control element. (f) Report about how the different sequences were obtained.

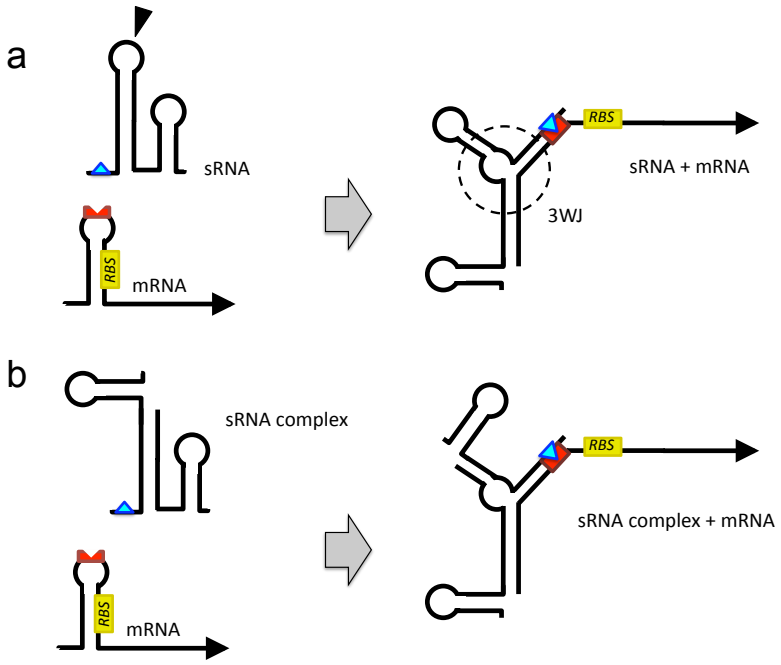

Figure S7: (a) Scheme of the riboregulatory system RAJ11 (one sRNA interacts with the 5' UTR of mRNA) [1]. (b) Scheme of the cooperative riboregulatory system trigR11 (two sRNAs form a complex that interacts with the 5' UTR). This system is based on the previous one by taking advantage of the three-way junction (3WJ) formed to then split the sRNA in two at the wedge (and add a terminator to the first fragment). The sRNAs are illustrated with terminators.

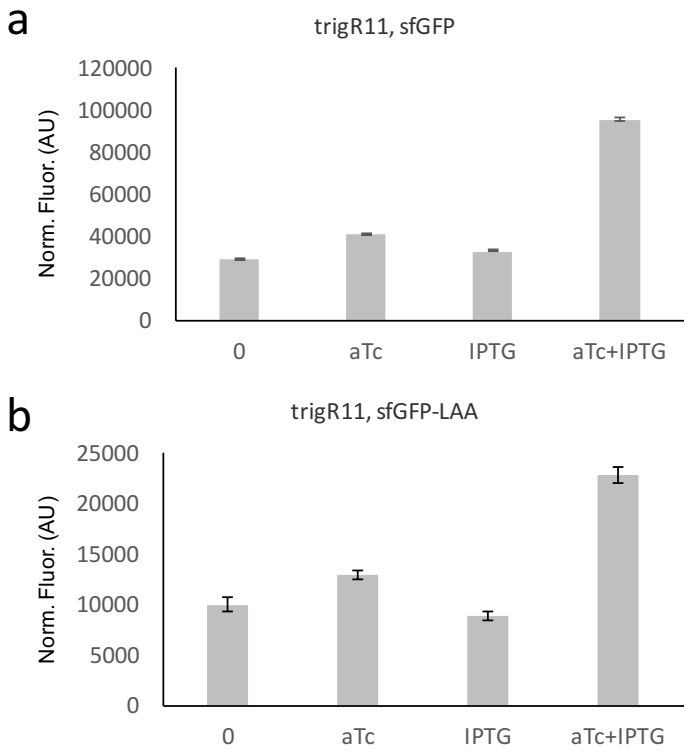

Figure S8: (a) Functional characterization of the designed sRNA system trigR11 with the reporter sfGFP without degradation tag. (b) Comparison against a recharacterization of that system in the same conditions using the tagged sfGFP (LAA). Three replicates. In those systems where the basal expression level is high (e.g., trigR2), a characterization with the non-tagged sfGFP gives non-significant differential expression due to saturation.

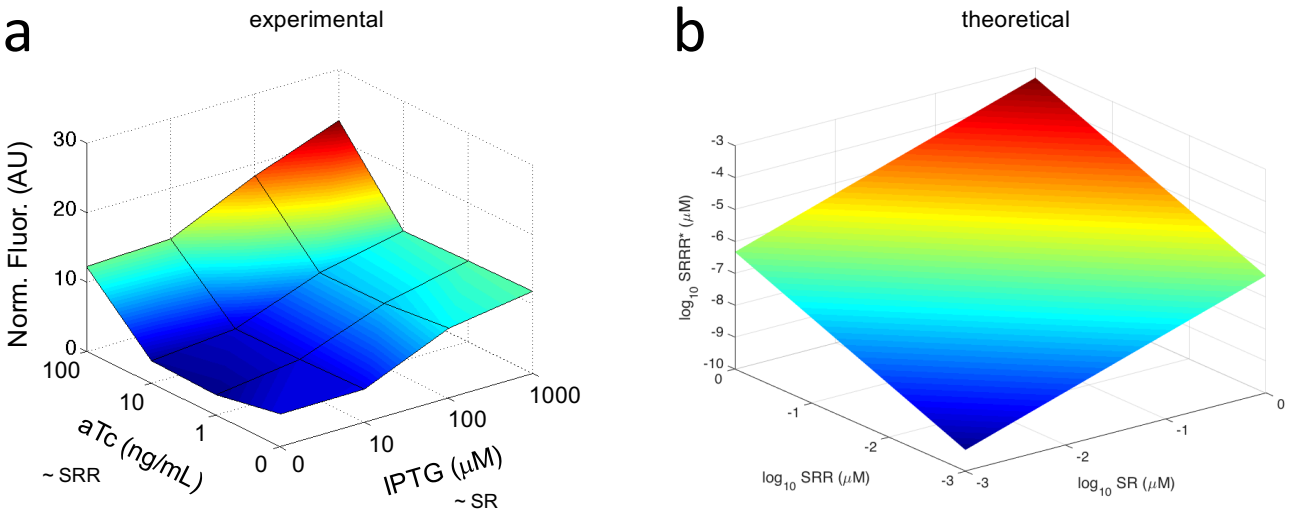

Figure S9: Effect of the concentrations of the sRNA molecules on the expression of the target gene. (a) For system trigR2, fluorescence results are shown for a gradient of IPTG and aTc. IPTG controls the expression of the sRNA SR, whilst aTc the expression of the sRNA SRR. (b) Model-based prediction of the formation of the complex SRRR* as a function of the concentration of the species SR and SRR, given a constant amount of the species SRRR (assumed 1 μM). See above *Equilibrium of RNA-RNA interactions*.

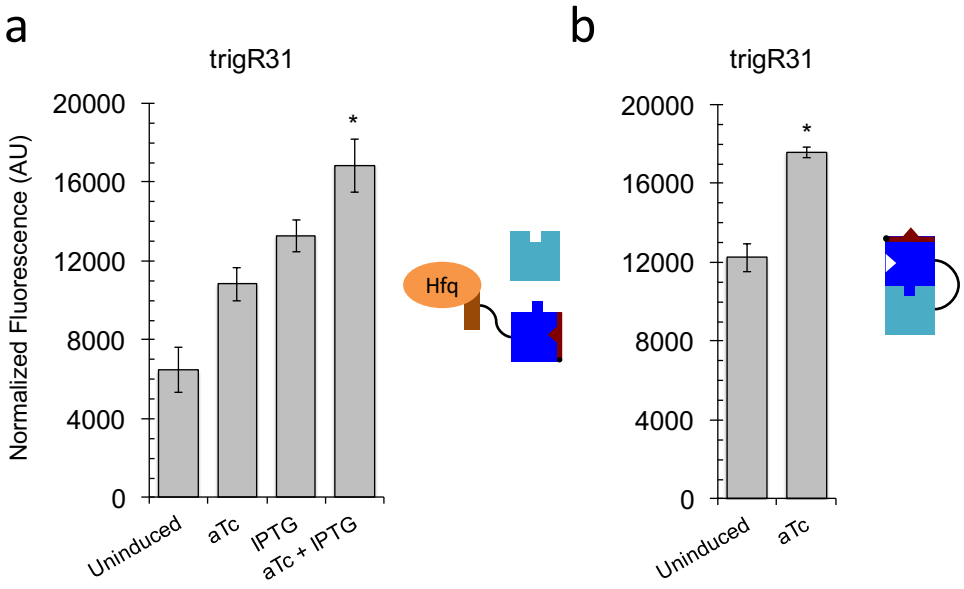

Figure S10: (a) Fluorescence results of two control systems based on trigR31 by introducing an Hfq scaffold in SRR, and by fusing transcriptionally the sRNAs SR and SRR. Three replicates. The differential expression is significant (one-tailed Welch *t*-test, $P < 0.05$; labeled with an asterisk).

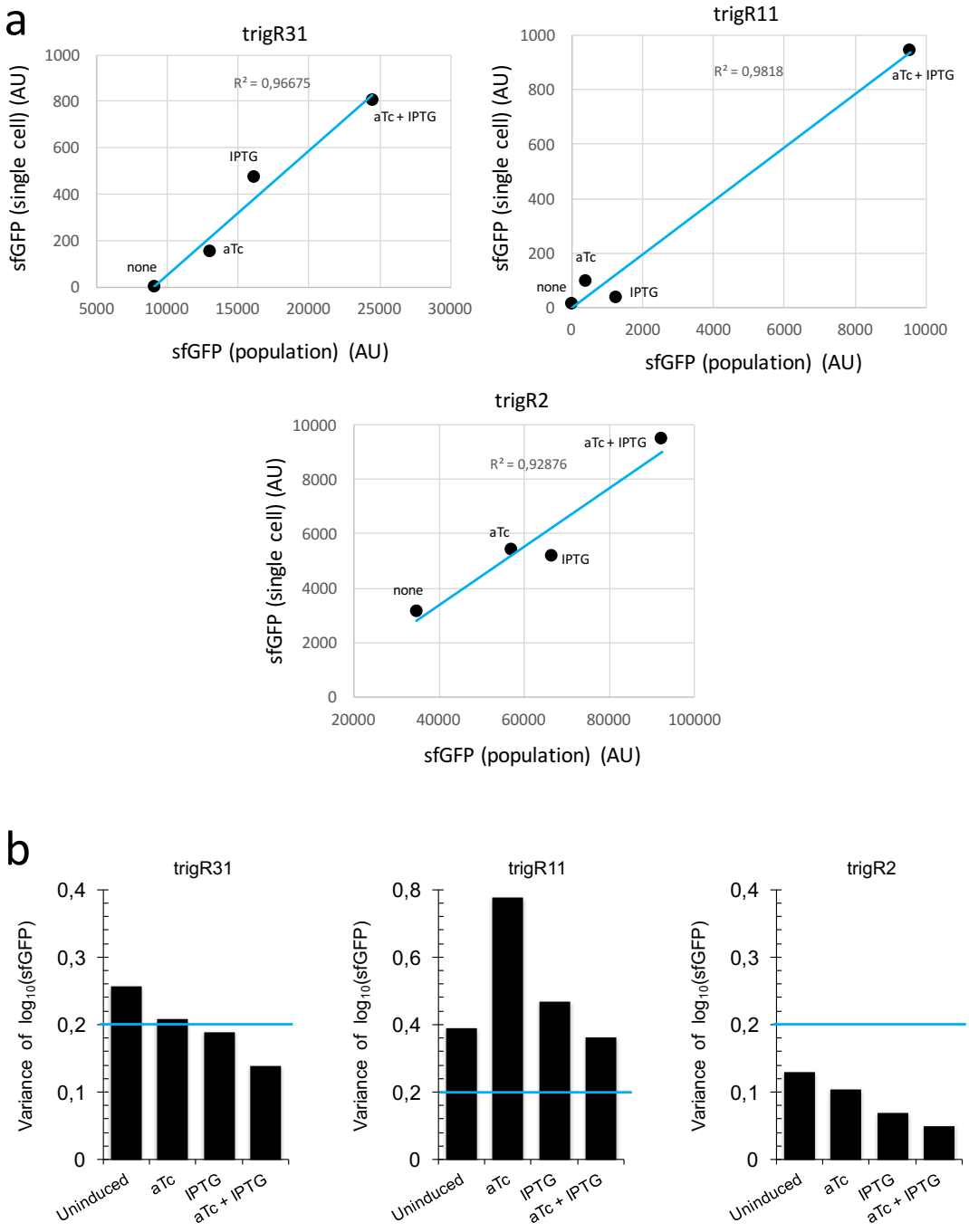

Figure S11: (a) Comparison between the activity of the designed sRNA systems trigR31, trigR11 and trigR2 at the population (by fluorometry, data for one clone) and single-cell levels (by flow cytometry, data for one clone). (b) Variance of sfGFP expression according to the single-cell data of the designed systems. The horizontal blue line corresponds to the variance reported for the system RAJ11 (simple riboregulation) upon induction [1] for a comparative.

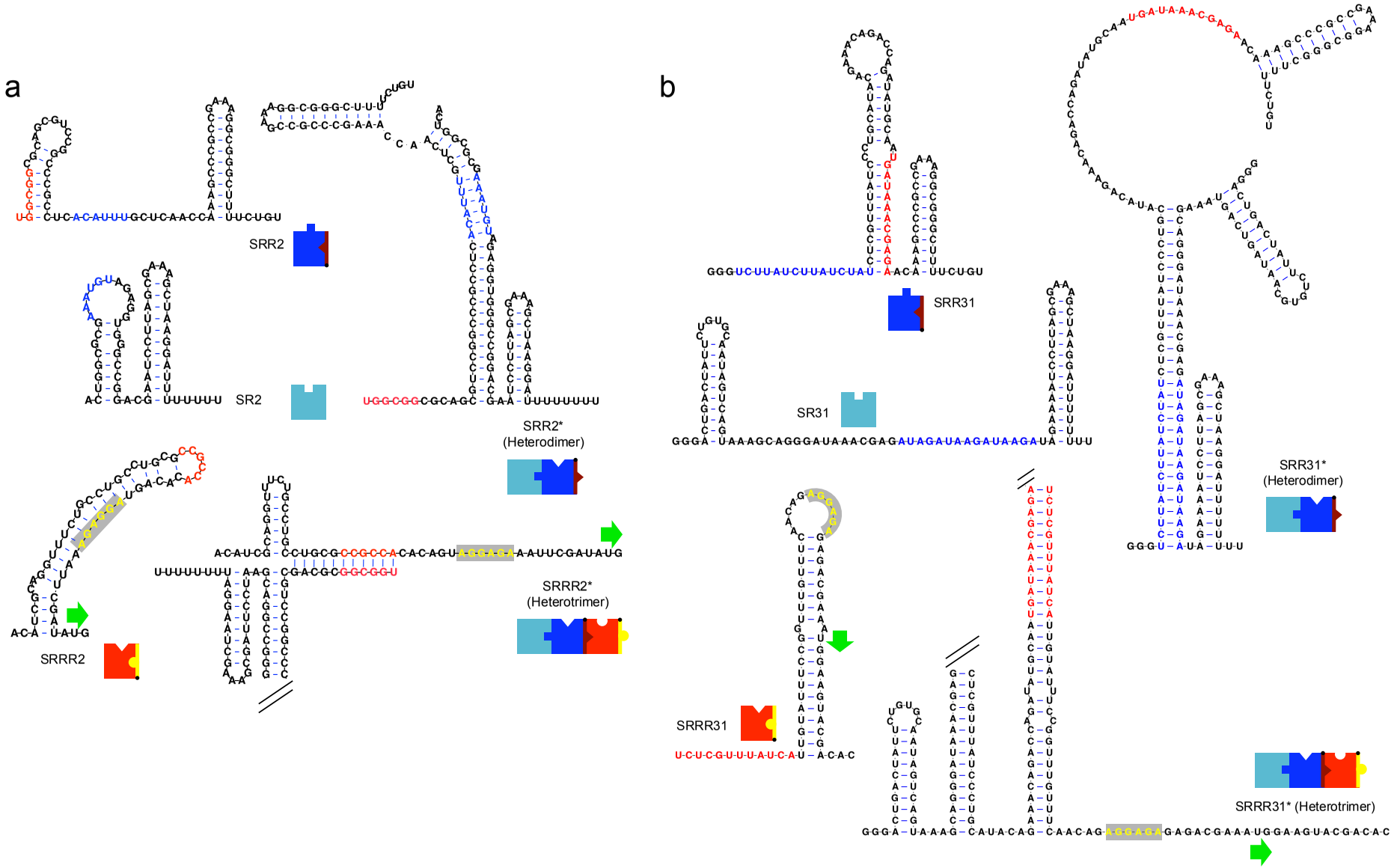
a
SRR2
SR2
SR2
SR2*
(Heterodimer)
SRRR2*
(Heterotrimer)
SRRR2
b
SRR31
SR31
SR31
SRR31*
(Heterodimer)
SRRR31
SRRR31* (Heterotrimer)

Figure S12: Sequences and structures of the species of the designed sRNA systems trigR2 (a) and trigR31 (b). The toehold for the interaction between the two sRNAs is shown in blue. The toehold for the interaction between the heterodimer (sRNA complex) and the 5' UTR is shown in red. In the 5' UTR (SRRR2 or SRRR31), the RBS is shown in yellow and the start codon marked by a green arrow. The transcription terminators T500 and TrrnC were used in SRR2 or SRR31 and in SR2 or SR31, respectively (see Table S1).

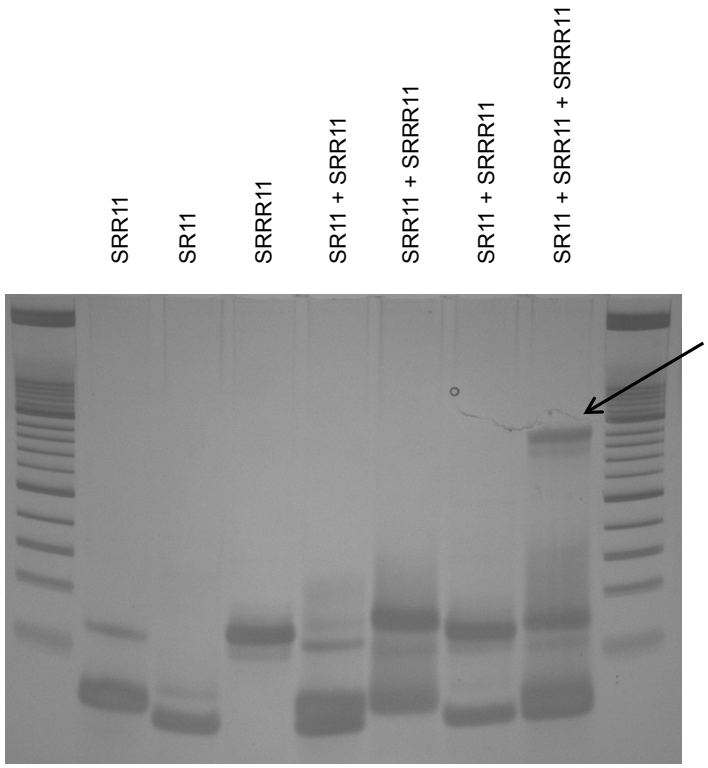

Figure S13: Electrophoretic analysis of system trigR11. The different lanes correspond to all combinations of species. The arrow marks the interaction of the three RNAs.

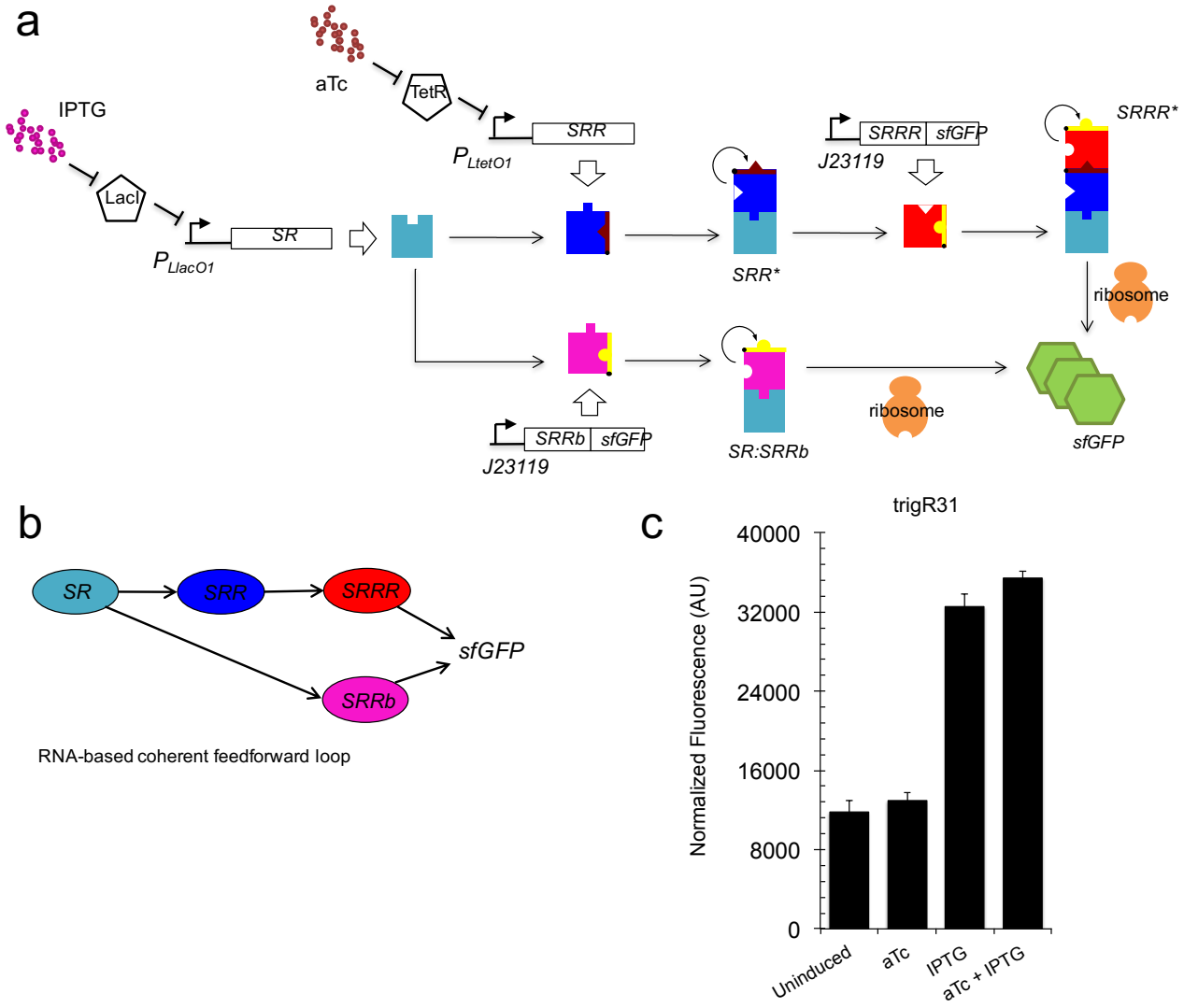

Figure S14. Functional characterization of designer feedforward loop gene circuit with riboregulatory cascades in bacterial cells. (a) Scheme of the engineered sRNA circuit. Promoters P_{LlacO1} and P_{LtetO1} control the expression of the two sRNAs (SR and SRR), which can be tuned with external inducers IPTG and aTc, whereas the two mRNAs (SRRR:sfGFP and SRRb:sfGFP) are constitutively expressed from promoter J23119. SR can directly activate one *cis*-repressed gene (SRRb:sfGFP), and the second *cis*-repressed gene (SRRR:sfGFP) is activated by the complex formed by the two sRNAs upon interaction (SRR*). The reporter gene is a sfGFP. (b) Minimal scheme of the feedforward loop circuit. (c) Fluorescence results (arbitrary units, AU) of the engineered circuit based on system trigR31 for all possible combinations of inducers. Error bars represent standard deviations over three replicates.

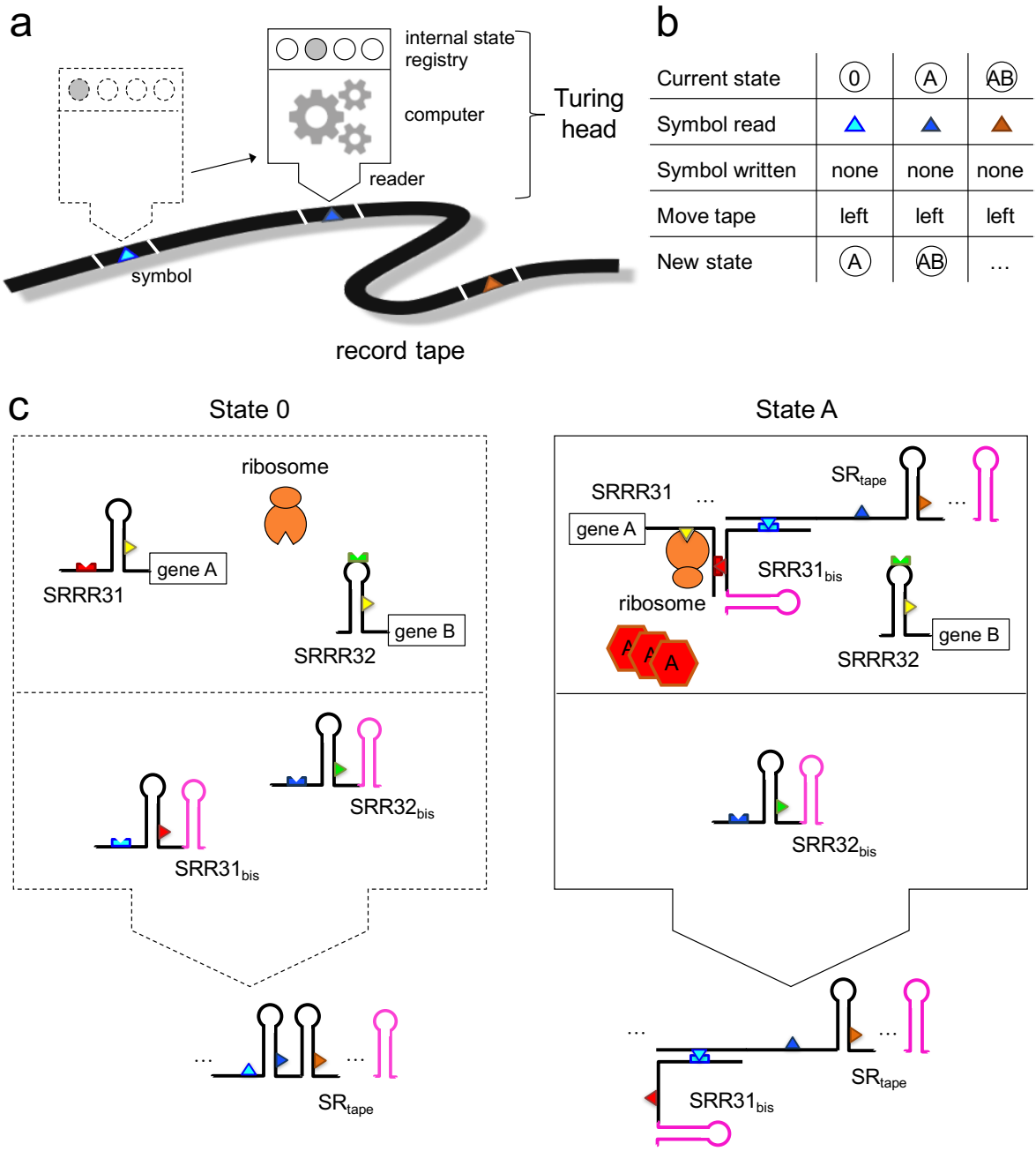

Figure S15. (a) General scheme of a Turing machine, where the head is positioned over the tape to read the symbols and then perform computations. Here, we consider a machine that reads but does not write on the tape. (b) Exemplification of a transition state table of the abstract machine. The instructions are implemented as 5-tuples, which given the current state of the machine and the symbol to be read in the tape dictate the new state of the machine, the symbol to be written instead, and the movement of the tape. (c) Implementation of the machine as an RNA hybridization network. We illustrate the transition from one state to another.

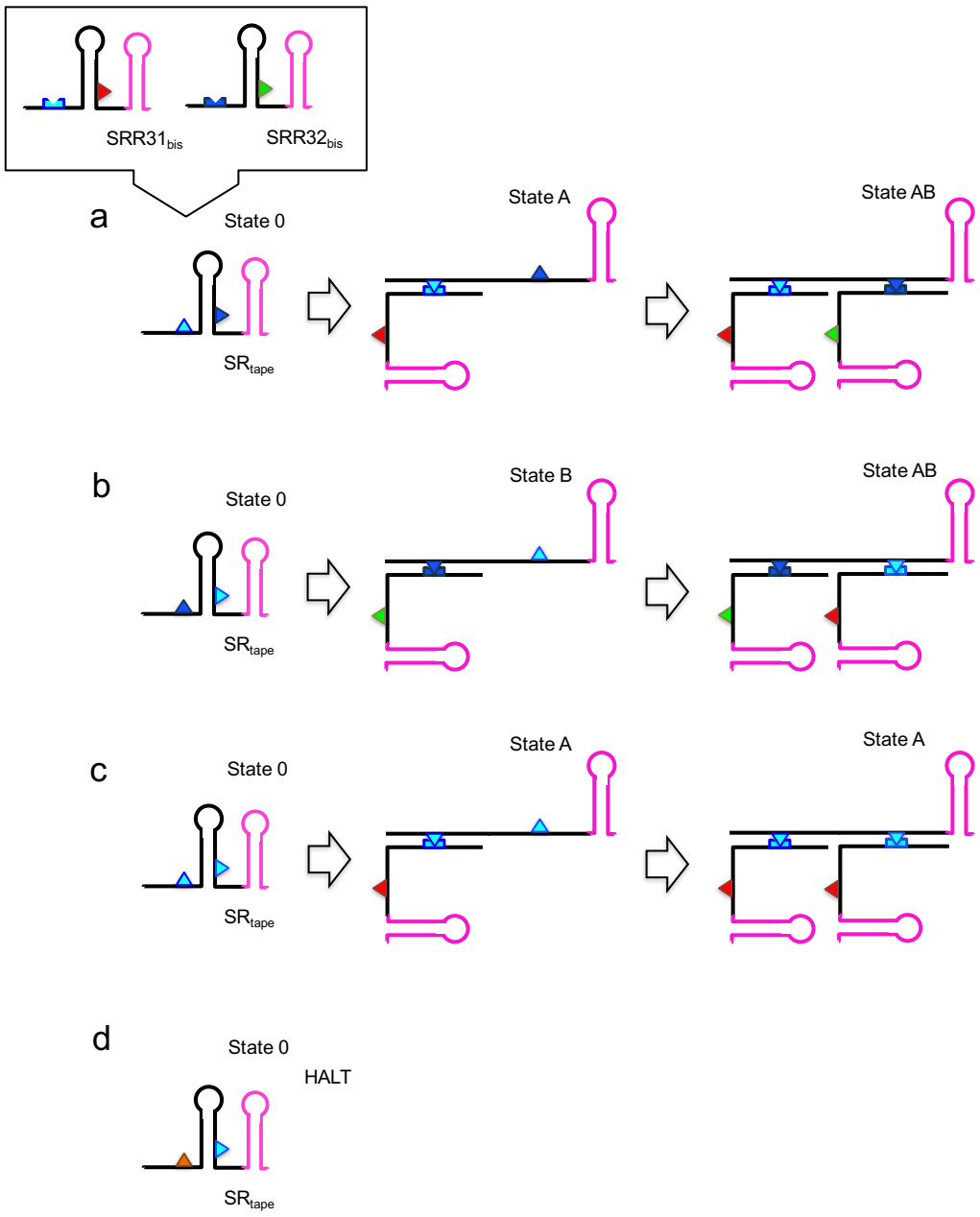

Current state	0	0	0	A	A	A	B	B	B
Symbol read	△	▲	▲	△	▲	▲	△	▲	▲
Symbol written	none	none	none	none	none	none	none	none	none
Move tape	left	left	HALT	left	left	HALT	left	left	HALT
New state	A	B	0	A	AB	A	AB	B	B

Figure S16. Illustration of how a Turing head implemented with two SRR molecules (here, $SRR31_{bis}$ and $SRR32_{bis}$) is able to read different tape molecules (appropriately designed). The Turing head also has a registry of the internal state implemented through SRRR molecules (here, SRRR31 and SRRR32), not shown for simplicity. On bottom, we show the transition state table of the machine.

Supplementary Tables

Table S1: Sequences of the RNA hybridization chain reactions designed in this work. Dot-bracket structures are also shown. The seed region for the interaction between the two sRNAs (SRR and SR) is shown in cyan. The seed region for the interaction between the sRNA complex and the 5' UTR (SRRR) is shown in red. In SRRR, the RBS is shown in yellow and the start codon in green. The transcription terminator T500 (efficiency > 90%) was used in SRR, shown in dark red, and the terminator TrrnC (efficiency > 90%) or B1002 (efficiency about 90%) in SR, shown in magenta (see ref. [27]).

System trigR2

>SRR2 (with T500)
UGGCGGCGCAGCGUCCGGCCCGCCUCACAUUUGCUCAACCAAAGCCCGCCGAAAGGCGGGCUUUUCU
GU
.(((((.((........)))))))..................((((((((((....))))))))))...
..

>SR2 (with TrrnC)
ACUGGCGCGAAAUGUAGAGGUGGGCCGGACGAAUCCUUAGCGAAAGCUAAGGAUUUUUUUU
.(((((.((...........)).)))))..((((((((((....))))))))))).....

>SRRR2
ACAUCGCAGGUUUCUGCCUGCCUGCGCCGCCACACAGUAGGAGAAAUUCGAUAUG
..((((..(((((((.(((((.((.(......).)))))))))))))))))...

System trigR1

>SRR1 (with T500)
AAUUUAGGCGGAGUUGGGUAGAGGACGCUGCUUGUACGCUCUCGUAUUGACGGCACCCGCGUCGAUG
UGAGGGACUUGGCAAAGCCCGCCGAAAGGCGGGCUUUUCUGU
....(((((((.(((........))).)))))))....((((((((((((.......))))))))))
))))))....((.((((((((((....))))))))))).))..

>SR1 (with B1002)
CAAGUCCGUGAAGUGUACGGGCAGCUUGAUAUUUCGACCCUACCAGUUGGAACUAUUAAUUUGGGAC
CAUUCAUAGUGGUUCCGAAGCGCAAAAAACCCCGCUUCGGCGGGGUUUUUUCGC
...(((((((.....)))))))...((((((((((((.......)))))))).)))))(((((((
((((...))))))))))))))((.((((((((((....))))))))))))

>SRRR1
AGUUCCGACGGGUCUCCUCUUUCGACUCCGCUUGAAAGAGGAGGUUUGUCAUAUG
......(((((..((((((((((((.....))))))))))))..)))))).....

System trigR11

>SRR11 (with T500)
GGGAGGGUUGAUUGUGUGAGUCUGUCACAGUUCAGCGGACAAAGCCCGCCGAAAGGCGGGCUUUUCU
GU
......(((((...(((((.....)))))..)))))).((.((((((((((....))))))))))).
..

>SR11 (with TrrnC)
AACGUUGAUGCUGUGACAGAUUUAUGCGAGGCAUCCUUAGCGAAAGCUAAGGAUUUUUUUU
........((((.((.((.....)))).)))))(((((((((....)))))))).........

>SRR11
CCUCGCAUAAUUUCACUUCUUCAAUCCUCCCGUUAAAGAGGAGAAAUUAUGAAUG
.....(((((((.(((((.(((.....))).)))))).)))))))).....

System trigR31

>SRR31 (with T500)
GGGUCUUAUCUUAUCUAUCUCGUUUAUCCCUGCAUACAGAAACAGACCAGAUAUGCAAUGAUAAACG
AGAACAAAGCCCGCCGAAAGGCGGGCUUUUCUGU
.................(((((((((((..(((((((.....).)))))))..)))))))))
))).((((((((((....))))))))))).....

>SR31 (with TrrnC)
GGGACUGACUAUUCUGUGCAAUAGUCAGUAAAGCAGGGAUAAACGAGAUAGAUAAGAUAAGAUAGAA
AAUCCUUAGCGAAAGCUAAGGAUUUUUUUU
...((((((((((.....))))))))).....................................((((
((((((((((....))))))))))))))..

>SRRR31
UCUCGUUUAUCAUUGUAUUUCCGGUUUGUUUCAACAGAGGAGAGAGACGAAAUGGAAGUACGACAC
............(((((((((((.(((((((.....)))))))).)))))))))))...

System trigR32

>SRR32 (with T500)
GGGUCACUUAAUCAUUUGUCGUCGUUUCUAUCUAUACAAGAACAGACCUCAUAUAGAAUGAAACGAC
GAAACCUGGCGGCAGCGCAAAAGAUGCGUAAACAAAGCCCGCCGAAAGGCGGGCUUUUCUGU
(.(((.............((((((((((..((((((..((.......))..))))))..)))))))))
)).....(((....))).....))).).....((((((((((....)))))))))).....

>SR32 (with TrrnC)
GGGUCGAGUAGACAGAGCUGUCUACUCGAAUAAGAUAGAAACGACGACAAAUGAUUAAGUGAGAAAU
CCUUAGCGAAAGCUAAGGAUUUUUUUU
...((((((((((....))))))))))).................................((((((
(((((((....)))))))))))))...

>SRRR32
ACGCAUUAUGUGCGUUGUCGCCCGUUUGUGUCUUUCAUUUCUAUAAUCAAAGGGAGUGGCAGUAUGU
AUAUGCGU
((((((((((((..(((((((.((((...................)))).)).)))))))))))
).))))))

Controls on system trigR31

>SRR31Hfq (Hfq scaffold in gray)
GGGUCUUAUCUUAUCUAUCUCGUUUAUCCCUGCAUACAGAAACAGACCAGAUAUGCAAUGAUAAACG
AGAACGUCCCGCAAGGAUGCGGGUCUGUUUACCCCUAUUUCAACCGGCCGCCUCGCGGCCGGUUUUU
UUUU
((((.............((((((((((..((((((.....).)))))).))))))))))
))).((.((((((....)))))).).....))))).......(((((((((...)))))))))...
....

>SRR31* (fusion; note that a 2-nt mutation was introduced to create a bulge in the large steam formed without affecting the free energies of interaction)
GGGACUGACUAUUCUGUGCAAUAGUCAGUAAAGCAGGGAUAAACGAGUAAGAUAAGAUAAGAUAGAA
AGGGUCUUAUCUUAUCUAUCUCGUUUAUCCCUGCAUACAGAAACAGACCAGAUAUGCAAUGAUAAAC
GAGAACAAAGCCCGCCGAAAGGCGGGCUUUUCUGU
...((((((((((.....))))))))))...(((((((((((((..((((((((((((....
...)))))))))))))..))))))))))))..((((..((...((....))...)).....
.....(((((((((....)))))))))))))

```
>SRRb31 (interacting with SR31)
GGGUCUUAUCUUAUCUAUCUCGUUUAUCCCUGCAUACAGAAACAGAGGAGAUAUGCAAUGAUAAACG
AGAACCUGGCGGCAGCGCAAAAGAUGCGUAAA
(.(((((.........(((((((((((..((((((.............).))))))..)))))))))
)))).....(((....)))..)))))).).....
```

Table S2: Strains and plasmids used in this work.

Strains or plasmids	**Features**	**Ref.**
E. coli DH5α	Commercial	Invitrogen
E. coli DH5α-Z1	Commercial (DH5α, *lacI*Q, PN25-*tetR*, SpR)	Clontech
E. coli MG1655-Z1	*lacI*Q, PN25-*tetR*, SpR	Gifted by M.B. Elowitz
ptrigR2	pSC101m ori, kanR, sfGFP-LAA	This work
ptrigR2St	pSC101m ori, kanR, sfGFP	This work
ptrigR1	pSC101m ori, kanR, sfGFP-LAA	This work
ptrigR11	pSC101m ori, kanR, sfGFP-LAA	This work
ptrigR11St	pSC101m ori, kanR, sfGFP	This work
ptrigR31	pSC101m ori, kanR, sfGFP-LAA	This work
ptrigR32	pSC101m ori, kanR, sfGFP-LAA	This work
pRAJ11	pUC ori, ampR-kanR, GFPmut3b	[1]
ptrigR31Hfq	pSC101m ori, kanR, sfGFP-LAA	This work
ptrigR31Fusion	pSC101m ori, kanR, sfGFP-LAA	This work
ptrigR11/2	sRNAs from system trigR11, 5' UTR from system trigR2 pSC101m ori, kanR, sfGFP-LAA	This work
ptrigR2/11	sRNAs from system trigR2, 5' UTR from system trigR11 pSC101m ori, kanR, sfGFP-LAA	This work
ptrigR31FFL	pUC ori, ampR, sfGFP-LAA (J23119:SRRb31)	This work

Table S3: Predicted values of the free energies of full hybridization (ΔG_1 and ΔG_2 for desired interactions, $\Delta \hat{G}_1$ and $\Delta \hat{G}_2$ for undesired ones) as well as toehold hybridization ($\Delta G_1^{\text{toehold}}$ and $\Delta G_2^{\text{toehold}}$ for desired interactions, $\Delta \hat{G}_1^{\text{toehold}}$ and $\Delta \hat{G}_2^{\text{toehold}}$ for undesired ones) for designer riboregulatory cascades. Also, predicted values of $\Delta G_{SRRR}^{\text{struct}}$ and $\Delta G_{SRRR*}^{\text{struct}}$ for those systems (calculated as previously done [2]). Values in Kcal/mol.

System	ΔG_1	$\Delta G_1^{\text{toehold}}$	ΔG_2	$\Delta G_2^{\text{toehold}}$
trigR31	-36.9	-17.9	-20.3	-11.2
trigR32	-30.1	-14.1	-18.6	-9.5
trigR1	-13.3	-4.8	-16.7	-9.5
trigR2	-23.9	-2.7	-19.3	-10.3
trigR11	-21.2	-2.3	-14.2	-10.3

$\Delta \hat{G}_1$	$\Delta \hat{G}_1^{\text{toehold}}$	$\Delta \hat{G}_2$	$\Delta \hat{G}_2^{\text{toehold}}$	$\Delta G_{SRRR}^{\text{struct}}$	$\Delta G_{SRRR*}^{\text{struct}}$
-15.6	-13.7	-20.9	0	1.2	0
-6.0	-3.4	-12.0	0	1.2	3.6
-5.6	0	-4.4	0	2.4	0
-3.1	0	-9.6	0	0	0
-8.6	0	-7.9	-10.3	2.4	0

Table S4. Cost of expressing the engineered sRNA systems in *E. coli*. The value of cell growth rate (h^{-1}), calculated by regressing OD_{600} with time during exponential phase (OD_{600} = 0.1 - 0.6), is shown for each induction condition. In brackets, the percentage of growth with respect to plain cells in the very same conditions.

	none	aTc	IPTG	aTc + IPTG
trigR31	0.2344 ± 0.0243 (97.3%)	0.2464 ± 0.0252 (102.3%)	0.1761 ± 0.0208 (73.1%)	0.1895 ± 0.0207 (78.7%)
trigR32	0.2665 ± 0.0096 (88.5%)	0.2728 ± 0.0017 (90.6%)	0.2201 ± 0.0042 (73.1%)	0.2233 ± 0.0041 (74.1%)
trigR1	0.3287 ± 0.0086 (99.9%)	0.3799 ± 0.0113 (115.4%)	0.3486 ± 0.0056 (105.9%)	0.3618 ± 0.0153 (109.9%)
trigR2	0.2975 ± 0.0202 (80.0%)	0.3106 ± 0.0216 (83.5%)	0.3033 ± 0.0203 (81.5%)	0.3246 ± 0.0152 (87.3%)
trigR11	0.2709 ± 0.0222 (69.7%)	0.2784 ± 0.0049 (71.6%)	0.2539 ± 0.0250 (65.3%)	0.2821 ± 0.0067 (72.6%)
trigR31FFL	0.2209 ± 0.0029 (86.3%)	0.2321 ± 0.0009 (90.6%)	0.1831 ± 0.0035 (71.5%)	0.1964 ± 0.0048 (76.7%)
plain cells	0.2408 ± 0.0022 0.3012 ± 0.0014 0.3291 ± 0.0029 0.3720 ± 0.0003 0.3886 ± 0.0068 0.2561 ± 0.0064	-	-	-

Table S5: Prediction of eventual off-target effect of the designed sRNAs using RNApredator [13]. Neighborhood of 90 nt before and 10 nt after the start codon (in *E. coli* K-12 MG1655). Essential genes bold-faced [28] (although the sRNAs do not hybridize with the RBSs of the essential genes targeted, expect SRR31 on *nusA*).

Riboregulator	**Potential target**
SRR2	*metH*
SR2	*mrcA, tusD, glpX, insH10, pyrF, arnA, clsC,* ***lptG****, yffL, entH*
SRR1	*rutC, adrA, ygeV, yfjR, melR*
SR1	*metB, rcsD, ykgE, gudX, ycbK*
SRR11	*ydfH, ttdT, yfiL, ydgD, melR, yegW, glpX, yicG,* ***hemH***
SR11	*dusB, phoB, iscU, yecE, phnD, sufC, yfcC, rimM*
SRR31	*insH11, quuD, rnc, ygaC,* ***rpsS****,* ***fbaA****,* ***nusA****, yhaM*
SR31	*yggI, quuD, mdtG, wcaE*
SRR32	*yggU, yafW, leuC*
SR32	*glgA, mprA, nfsB, yccS, rihA, phnP, ybjG, ybaY,* ***cdsA***

Table S6: Additional sequences for the theoretical design of an RNA-based computer. Dot-bracket structures are also shown.

>SRtape (with TrrnC)

```
GGGACUGACUAUUCUGUGCAAUAGUCAGUAAAGCAGGGAUAAACGAGAUAGAUAAGAUAAGAUAGAA
ACGUGGCGACGUUUCUAUCUUAUCUGUAAGUGACCAUCCUUAGCGAAAGCUAAGGAUUUUUUUU
...((((((((((......))))))))))).........................((((((((((((
((((....))))))))))))))))).........(((((((((....)))))))))).......
```

>SRR31bis (with T500)

```
ACGUUUCUAUCUUAUCUUAUCUAUCUCGUUUAUCCCUGCAUACAGAAACAGACCAGAUAUGCAAUGA
UAAACGAGAACAAAGCCCGCCGAAAGGCGGGCUUUUCUGU
.......................((((((((((..((((((.............))))))..))
)))))))))..((((((((((....))))))))))).....
```

>SRR32bis (with T500)

```
UAUAAACGAGAUAGGUUAUUUAAAGAUAAGAUCGUCGCCUCGACUAUAAAAGAACAGACCUCAUAUA
GAAUGAAACGACGAAACCUGGCGGCAGCGCAAAAGAUGCGUAAACAAAGCCCGCCGAAAGGCGGGCU
UUUCUGU
......((...((((((.............((((((..(((.(((((..((.......))..))))
)..))))..))))))))))).))...(((((.....)))))....((((((((((....))))))))
))).....
```

Supplementary References

[1] Rodrigo, G., Landrain, T.E., & Jaramillo, A. De novo automated design of small RNA circuits for engineering synthetic riboregulation in living cells. *Proc. Natl. Acad. Sci. USA* 109, 15271-15276 (2012).

[2] Rodrigo, G., Landrain, T.E., Majer, E., Daròs, J.-A., & Jaramillo, A. Full design automation of multi-state RNA devices to program gene expression using energy-based optimization. *PLoS Comput. Biol*. 9, e1003172 (2013).

[3] Hofacker, I.L., Fontana, W., Stadler, P.F., Bonhoeffer, L.S., Tacker, M., & Schuster, P. Fast folding and comparison of RNA secondary structures. *Monatsh. Chem.* 125, 167-188 (1994).

[4] Salis, H.M., Mirsky, E.A., & Voigt, C.A. Automated design of synthetic ribosome binding sites to control protein expression. *Nat. Biotechnol.* 27, 946-950 (2009).

[5] Green, A.A., Silver, P.A., Collins, J.J., & Yin, P. Toehold switches: de-novo-designed regulators of gene expression. *Cell* 159, 925-939 (2014).

[6] Schindelin, J., Arganda-Carreras, I., Frise, E., *et al.* Fiji: an open-source platform for biological-image analysis. *Nat. Methods* 9, 676-682 (2012).

[7] Phillips, R. Napoleon is in equilibrium. *Annu. Rev. Condens. Matter Phys.* 6, 85-111 (2015).

[8] Lutz, R., & Bujard, H. Independent and tight regulation of transcriptional units in Escherichia coli via the LacR/O, the TetR/O and AraC/I1-I2 regulatory elements. *Nucleic Acids Res.* 25, 1203-1210 (1997).

[9] Rodrigo, G., Majer, E., Prakash, S., Daros, J.A., Jaramillo, A., & Poyatos, J.F. Exploring the dynamics and mutational landscape of riboregulation with a minimal synthetic circuit in living cells. *Biophys. J.* 109, 1070-1076 (2015).

[10] Soper, T., Mandin, P., Majdalani, N., Gottesman, S., & Woodson, S.A. Positive regulation by small RNAs and the role of Hfq. *Proc. Natl. Acad. Sci. USA* 107, 9602-9607 (2010).

[11] Sakai, Y., Abe, K., Nakashima, S., Yoshida, W., Ferri, S., Sode, K., & Ikebukuro, K. Improving the gene-regulation ability of small RNAs by scaffold engineering in Escherichia coli. *ACS Synth. Biol.* 3, 152-162 (2014).

[12] Adamson, D.N., & Lim, H.N. Essential requirements for robust signaling in Hfq dependent small RNA networks. *PLoS Comput. Biol*. 7, e1002138 (2011).

[13] Eggenhofer, F., Tafer, H., Stadler, P.F., & Hofacker, I.L. RNApredator: Fast accessibility-based prediction of sRNA targets. *Nucleic Acids Res.* 39, W149-W154 (2011).

[14] Turing, A.M. On computable numbers, with an application to the Entscheidungsproblem. *Proc. Lond. Math. Soc.* 42, 230-265 (1936).

[15] Adleman, L.M. Molecular computation of solutions to combinatorial problems. *Science* 266, 1021-1024 (1994).

[16] Benenson, Y., Paz-Elizur, T., Adar, R., Keinan, E., Livneh, Z., & Shapiro, E. Programmable and autonomous computing machine made of biomolecules. *Nature* 414, 430-434 (2001).

[17] Shapiro, E., & Benenson, Y. Bringing DNA computers to life. *Sci. Am.* 294, 44-51 (2006).

[18] Amos, M., Axmann, I., Bluethgen, N., de la Cruz, F., Jaramillo, A., Rodriguez-Paton, A., & Simmel, F. Bacterial computing with engineered populations. *Phil. Trans. R. Soc. A* 373, 20140218 (2015).

[19] Regot, S., Macia, J., Conde, N., Furukawa, K., *et al*. Distributed biological computation with multicellular engineered networks. *Nature* 469, 207-211 (2011).

[20] Roquet, N., Soleimany, A.P., Ferris, A.C., Aaronson, S., & Lu, T.K. Synthetic recombinase-based state machines in living cells. *Science* 353, aad8559 (2016).

[21] Shipman, S.L., Nivala, J., Macklis, J.D., & Church, G.M. Molecular recordings by directed CRISPR spacer acquisition. *Science* 353, aaf1175 (2016).

[22] Liu, C.C., Qi, L., Lucks, J.B., Segall-Shapiro, T.H., Wang, D., Mutalik, V.K., & Arkin, A.P. An adaptor from translational to transcriptional control enables predictable assembly of complex regulation. *Nat. Methods* 9, 1088-1094 (2012).

[23] Qi, L.S., Larson, M.H., Gilbert, L.A., Doudna, J.A., Weissman, J.S., Arkin, A.P., & Lim, W.A. Repurposing CRISPR as an RNA-guided platform for sequence-specific control of gene expression. *Cell* 152, 1173-1183 (2013).

[24] Roth, A., Weinberg, Z., Chen, A.G.Y., Kim, P.B., Ames, T.D., & Breaker, R.R. A widespread self-cleaving ribozyme class is revealed by bioinformatics. *Nat. Chem. Biol.* 10, 56-60 (2013).

[25] Vogel, J., Bartels, V., Tang, T.H., Churakov, G., Slagter-Jager, J.G., Huttenhofer, A., & Wagner, E.G.H. RNomics in Escherichia coli detects new sRNA species and indicates parallel transcriptional output in bacteria. *Nucleic Acids Res.* 31, 6435-6443 (2003).

[26] Bennett, M.R., & Hasty, J. Microfluidic devices for measuring gene network dynamics in single cells. *Nat. Rev. Genet*. 10, 628-638 (2009).

[27] Rostain, W., Landrain, T.E., Rodrigo, G., & Jaramillo, A. Regulatory RNA design through evolutionary computation and strand displacement. *Methods Mol. Biol.* 1244, 63-78 (2015).

[28] Yamazaki, Y., Niki, H., & Kato, J. Profiling of Escherichia coli chromosome database. *Methods Mol. Biol*. 416, 385-389 (2008).